

Entanglement Rényi Negativity of Interacting Fermions from Quantum Monte Carlo Simulations

Fo-Hong Wang¹ and Xiao Yan Xu^{1,2,*}

¹Key Laboratory of Artificial Structures and Quantum Control (Ministry of Education), School of Physics and Astronomy, Shanghai Jiao Tong University, Shanghai 200240, China

²Hefei National Laboratory, Hefei 230088, China

(Dated: April 30, 2024)

Many-body entanglement unveils additional aspects of quantum matter and offers insights into strongly correlated physics. While ground-state entanglement has received much attention in the past decade, the study of mixed-state quantum entanglement using negativity in interacting fermionic systems remains largely unexplored. We demonstrate that the partially transposed density matrix of interacting fermions, similar to their reduced density matrix, can be expressed as a weighted sum of Gaussian states describing free fermions, enabling the calculation of rank- n Rényi negativity within the determinant quantum Monte Carlo framework. We conduct the first calculation of rank-two Rényi negativity for the half-filled Hubbard model and the spinless t - V model and find that the area law coefficient of the Rényi negativity has a logarithmic finite-size scaling at the finite-temperature transition point. Our work contributes to the calculation of entanglement and sets the stage for future studies on quantum entanglement in various fermionic many-body mixed states.

Introduction.—The characterization of emerging quantum many-body phenomena is multifaceted. Traditionally, physicists have relied on local measurements based on linear response to investigate matter. In recent decades, the utilization of quantum entanglement, a fundamental concept in quantum physics and a powerful tool in quantum information, has become pivotal in unveiling the additional aspects of quantum matter, including the identification of exotic phases and quantum criticality [1–3]. A prominent example is the entanglement entropy (EE) used in bipartite ground-state entanglement studies [4], where various corrections to the area law [5–7] have been employed to classify quantum phases. These include logarithmic corrections in the leading area-law term for 1D critical systems [8, 9] and Fermi surfaces in generic dimensions [10–12], subleading logarithmic terms for corner contributions to 2D critical systems [13, 14] and Goldstone modes in symmetry-breaking phases [15–18], and the topological EE for non-local orders [19–23].

However, EE is not a faithful mixed-state entanglement measurement due to its incompetence in distinguishing quantum entanglement from classical correlation. Thus, many entanglement measurements for mixed states have been proposed [24, 25], including the entanglement negativity [26–29] (referred to as “negativity” henceforth for brevity), which was designed base on positive partial transpose criteria for the separability of density matrices [30, 31]. The evaluation of negativity hinges on the partial transpose of the given density matrix and can be carried out straightforwardly through basic matrix manipulations without invoking any optimization. Hence, negativity has been employed to examine entanglement in finite-temperature Gibbs states or tripartite ground states in various systems, spanning from one-dimensional conformal field theory [32–35], bosonic

systems [36–40], spin systems [41–47], to topologically ordered phases [48–53].

In the case of fermionic systems, the definition of partial transpose needs to be adjusted to accommodate the anticommuting statistical property. There exist two different proposals for fermionic partial transpose and corresponding fermionic negativity, as discussed in Refs. [54, 55] and Refs. [56–58] respectively. Despite being a “computable entanglement measurement”, fermionic negativity is only analytically tractable in free systems, especially at finite temperatures, and there have been studies based on both the former definition [39, 59–61] and the latter definition [56, 62–65]. Therefore, it is desirable to design a quantum Monte Carlo (QMC) algorithm for large-scale simulation of interacting fermionic systems in an unbiased manner, which is the main goal of this letter. Throughout this paper, we adopt the definition in Refs. [56, 57] under which the partial transpose of a Gaussian state remains a Gaussian state. Additionally, instead of utilizing the originally proposed negativity which involves trace norm of partially transposed density matrices (PTDMs) [28], we consider Rényi negativity which involves moments of PTDMs, as done in several previous studies on other systems [32, 33, 37, 39, 40, 45, 47].

In fact, our main result is more broadly applicable. We show that generic PTDMs can be written as a weighted sum of Gaussian states, representing free fermions coupled with auxiliary fields, similar to Grover’s pioneering work on reduced density matrices for EE [66]. Our finding facilitates the calculation of Rényi negativity in a tractable manner, thus establishing it as a powerful tool for characterizing entanglement in mixed states of interacting fermions. We demonstrate this relation using determinant quantum Monte Carlo (DQMC) simulations [67–69] on two paradigmatic models in the realm

of strongly correlated electrons, namely, the Hubbard model and the spinless t - V model. These two models on bipartite lattices at half-filling are sign-problem-free and both ground-state and finite-temperature properties can be feasibly simulated within the DQMC framework. The relation between negativity and finite temperature transition in fermionic systems is unveiled.

Partially transposed density matrix in DQMC calculations.—Various definitions of negativity in the literature share a common and central dependency, namely, the partial transpose of the density matrix. In this work, we adopt the partial time-reversal transformation proposed by Shapourian *et al.* [56, 57] as the fermionic partial transpose.

We begin with the general partitioning of a fermionic lattice model. It is defined using annihilation (creation) operators $c_{j\sigma}^{(\dagger)}$, which satisfy the anticommutation relations $\{c_{j\sigma}, c_{k\sigma'}^\dagger\} = \delta_{jk}\delta_{\sigma\sigma'}$, where $j, k = 1, \dots, N$ are the labels of the sites and σ, σ' are the indices for internal degrees of freedom such as spin. This lattice system, denoted as A , generally exists within a larger space. After tracing out the environment \bar{A} , system A typically exists in a mixed state ρ . For example, if system A is in contact with a much larger thermal bath at temperature T , then we obtain a finite-temperature Gibbs state $\rho = e^{-\beta H} / \text{Tr} e^{-\beta H}$ with $\beta = 1/T$ the inverse temperature and H the Hamiltonian of the system A . Next, we further divide system A into two parties belonging to two complementary spatial regions respectively, i.e., $A = A_1 \cup A_2$. Then the density matrix acting on Hilbert space $\mathcal{H}_1 \otimes \mathcal{H}_2$ can be expanded as $\rho = \sum_{A_1, A_2, A'_1, A'_2} \rho_{A_1, A_2; A'_1, A'_2} |A_1\rangle |A_2\rangle \langle A'_1| \langle A'_2|$.

The fermionic partial transpose of density matrix ρ with respect to subsystem A_2 , denoted as $\rho^{T_2^f}$, exhibits a highly succinct mathematical expression in the Majorana basis [56, 57, 70]. Under Majorana basis, an arbitrary density operator can be expressed as a constrained superposition of products of Majorana operators, which are defined as $\gamma_{2j-1, \sigma} = c_{j, \sigma} + c_{j, \sigma}^\dagger$ and $\gamma_{2j, \sigma} = -i(c_{j, \sigma} - c_{j, \sigma}^\dagger)$. It is found that $\rho^{T_2^f}$ can be obtained by applying the following transformation to the Majorana operators associated with subsystem A_2 :

$$\mathcal{R}_2^f(\gamma_{j, \sigma}) = i\gamma_{j, \sigma}, \quad j \in A_2. \quad (1)$$

Remarkably, under this definition, the fermionic partial transpose of a Gaussian state, denoted as $\rho_0 \sim e^{\frac{1}{4}\gamma^T W \gamma}$, retains its Gaussian nature. The question then pertains to determining the explicit form of $\rho_0^{T_2^f}$ or $W^{T_2^f}$. To this end, it is important to emphasize that a Gaussian state ρ_0 can be alternatively characterized by the Green's function $\Gamma_{kl} = \langle [\gamma_k, \gamma_l] \rangle / 2$, which is averaged with respect to ρ_0 itself and also called covariance matrix. This matrix is connected to the W matrix through the relations $\tanh(-W/2) = \Gamma$ [54, 70]. By employing the definition

of Γ and the partial transpose in the Majorana basis (refer to Eq. (1)), the partial transpose of the covariance matrix can be formulated as

$$\Gamma^{T_2^f} = \begin{pmatrix} \Gamma^{11} & i\Gamma^{12} \\ i\Gamma^{21} & -\Gamma^{22} \end{pmatrix}, \quad (2)$$

where $\Gamma^{bb'}$ ($b, b' = 1, 2$) denotes the block comprising the matrix elements with rows pertaining to subsystem A_b and columns pertaining to subsystem $A_{b'}$. The Gaussian state described by $\Gamma^{T_2^f}$ precisely yields the $\rho_0^{T_2^f}$ through $\tanh(-W^{T_2^f}/2) = \Gamma^{T_2^f}$ [77].

The above discussion in the Majorana basis can be seamlessly transitioned to the complex fermion basis. In complex fermion basis, the Green's function is defined as $G_{jk} = \langle c_j c_k^\dagger \rangle$, where we have abbreviated the spin indices. Its partially transposed form exhibits also a simple structure

$$G^{T_2^f} = \begin{pmatrix} G^{11} & iG^{12} \\ iG^{21} & I - G^{22} \end{pmatrix}, \quad (3)$$

where the superscripts of the blocks $G^{bb'}$ indicate the subsystems, akin to the notation of $\Gamma^{bb'}$ established earlier. Similar to the Majorana basis, the above Green's function delineates another Gaussian state which is exactly the partial transpose of the original Gaussian state, i.e., $(\rho_0[G])^{T_2^f} = \rho_0[G^{T_2^f}]$ with $\rho_0[G] \sim e^{\mathbf{c}^\dagger \ln(G^{-1} - I)\mathbf{c}}$ [78].

It is now pertinent to redirect our attention towards the partial transpose for interacting fermionic systems, whose density matrices are not Gaussian states. Nonetheless, within the framework of DQMC, after Trotter decomposition and Hubbard-Stratonovich decoupling [70], the original two-particle interaction terms are replaced by fermion bilinears coupled with spacetime-dependent auxiliary fields \mathbf{s} . The partition function is given by $Z = \sum_{\mathbf{s}} \text{Tr} [\prod_{l=1}^{L_\tau} e^{\mathbf{c}^\dagger K_l[\mathbf{s}] \mathbf{c}}]$, where L_τ is the number of time slices and $\mathbf{c} = (c_1, \dots, c_N)^T$ (for simplicity we abbreviate spin indices). The density matrix ρ can also be expressed as a weighted sum of Gaussian operators, explicitly $\rho = \sum_{\mathbf{s}} P_{\mathbf{s}} \rho_{\mathbf{s}}$ with $P_{\mathbf{s}}$ representing the weight of configuration \mathbf{s} [66, 70]. After partial transpose, it takes the form

$$\rho^{T_2^f} = \sum_{\mathbf{s}} P_{\mathbf{s}} \rho_{\mathbf{s}}^{T_2^f}, \quad (4)$$

where

$$\rho_{\mathbf{s}}^{T_2^f} = \det [G_{\mathbf{s}}^{T_2^f}] \exp \left\{ \mathbf{c}^\dagger \ln \left[\left(G_{\mathbf{s}}^{T_2^f} \right)^{-1} - I \right] \mathbf{c} \right\}. \quad (5)$$

The aforementioned equations (4) and (5), along with Eq. (3), are the main result of this letter and can be employed to investigate negativity and negativity spectrum within the conventional DQMC framework, fully analogous to the analysis of EE and entanglement spectrum, respectively.

Rényi negativity for Hubbard chain.— We consider the half-filled Hubbard chain with periodic boundary conditions, described by the Hamiltonian

$$H = -t \sum_{\langle ij \rangle \sigma} (c_{i\sigma}^\dagger c_{j\sigma} + \text{H.c.}) + \frac{U}{2} \sum_i (n_i - 1)^2, \quad (6)$$

which is a sign-problem-free model [69, 70]. We will benchmark DQMC results from two perspectives: (i) a numerical comparison with results obtained from exact diagonalization [79], and (ii) providing a physical explanation for why the negativity is a more competent mixed-state entanglement measurement compared to EE in the context of a quantum-classical crossover [56, 62].

We define the rank- n Rényi negativity as

$$\mathcal{E}_n = -\frac{1}{n-1} \ln \text{Tr} \left[\left(\rho^{T_2^f} \right)^n \right], \quad (7)$$

where the n -th moment of the PTDM, denoted as $\text{Tr}[(\rho^{T_2^f})^n]$ [80], is also referred to as the replica approach of negativity in previous studies [32, 33]. The quantity \mathcal{E}_n is formally a direct analog to rank- n Rényi EE $S_n(A_1) = -(\ln \text{Tr} \rho_{A_1}^n)/(n-1)$, where $\rho_{A_1} = \text{Tr}_{A_2} \rho$ represents the reduced density operator obtained after tracing out subsystem A_2 . Utilizing Eq. (4), we can derive the DQMC expression for measuring, for instance, the rank-two Rényi negativity,

$$\mathcal{E}_2 = -\ln \left\{ \sum_{\mathbf{s}_1 \mathbf{s}_2} P_{\mathbf{s}_1} P_{\mathbf{s}_2} \times \det \left[G_{\mathbf{s}_1}^{T_2^f} G_{\mathbf{s}_2}^{T_2^f} + \left(I - G_{\mathbf{s}_1}^{T_2^f} \right) \left(I - G_{\mathbf{s}_2}^{T_2^f} \right) \right] \right\} \quad (8)$$

The distinction between the fermionic partial transpose and the conventional one is presented herein. For bosonic systems, considering that $\text{Tr}[(\rho^{T_2})^2] = \text{Tr}[\rho^2]$, the rank-two Rényi negativity becomes trivial, thereby rendering the minimal meaningful rank as three [32, 33, 47]. However, we show in the occupation number representation that all fermionic PTDMs satisfy $\text{Tr}[(\rho^{T_2^f})^2] = \text{Tr}[(\hat{X}_2(\pi))^2]$ with $\hat{X}_2(\theta) = e^{i\theta \sum_{j \in A_2} n_j}$ being the disorder operator [70]. Consequently, \mathcal{E}_2 can reveal the entanglement information of the system. As shown in Fig. 1, the results calculated by DQMC and exact diagonalization show strong agreement in both the zero-temperature and finite-temperature regimes. In the zero-temperature regime, the pattern of the rank-two Rényi negativity exhibits analogous variations to those of the rank-two Rényi EE [66, 81], in response to alterations in the length of subsystem A_1 , denoted as L_{A_1} . However, at finite temperatures, the negativity maintains a symmetric pattern, which is different from the behavior of EE [81, 82]. As the temperature rises, the magnitude of the negativity increases, resulting in an overall non-zero shift corresponding to a non-zero thermodynamic entropy of $-\ln(\text{Tr} \rho^2)$.

Based on the above observation in finite-temperature regime, we also examine the ratio between $\text{Tr}[(\rho^{T_2^f})^n]$ and

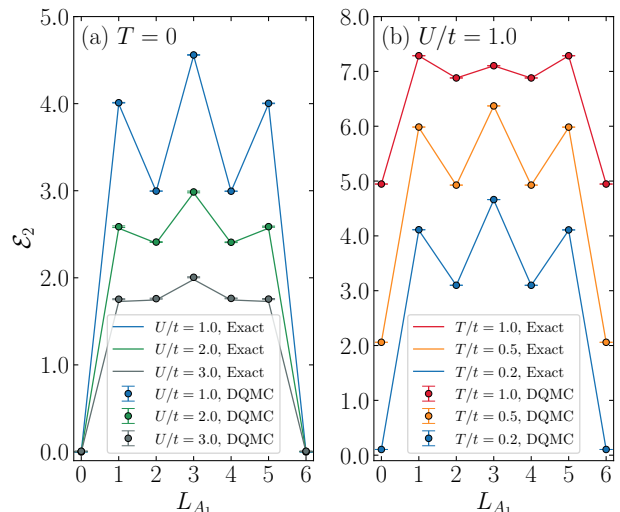


FIG. 1. The variation of the rank-two Rényi negativity \mathcal{E}_2 for a six-site Hubbard chain with periodic boundary conditions is depicted as a function of the subsystem length L_{A_1} . The solid lines represent the exact diagonalization results, which agree with the DQMC results at both (a) zero temperature and (b) finite temperatures.

$\text{Tr}[\rho^n]$ as previous Monte Carlo investigations on bosonic systems [37, 45, 47]

$$R_n = -\frac{1}{n-1} \ln \left\{ \frac{\text{Tr} \left[\left(\rho^{T_2^f} \right)^n \right]}{\text{Tr}[\rho^n]} \right\} = \mathcal{E}_n - S_n^{\text{th}}, \quad (9)$$

where $S_n^{\text{th}} = -(\ln \text{Tr} \rho^n)/(n-1)$ represents the thermodynamic Rényi entropy, which can be computed by considering the subsystem A_2 as non-existent in \mathcal{E}_n . The faithful description of mixed-state entanglement necessitates the subtraction of the thermodynamic Rényi entropy S_n^{th} from the Rényi negativity \mathcal{E}_n . In Fig. 2, we display the variations of the negativity ratio and EE with temperature for three distinct lengths, namely $L = 6, 10, 14$. Here, the subsystem A_1 is selected to be half of the chain, yielding an equal bipartition. As the temperature rises, the EE increases while the negativity ratio asymptotically diminishes to zero for all lengths. This serves as a compelling physical demonstration of the Rényi negativity ratio. In a generic mixed state, both quantum and classical correlations are present, and effective measurement of mixed-state entanglement should exclusively isolate the quantum correlations [28]. In the specific context of finite-temperature Gibbs states, the classical correlation is simply the thermal fluctuations delineated by the thermodynamic entropy S_n^{th} . Furthermore, at sufficiently low temperatures, the negativity ratio remains constant and establishes a plateau, the length of which is associated with the finite-size gap $1/L$ [62]. As depicted in Fig. 2, it is evident that with an increase in chain

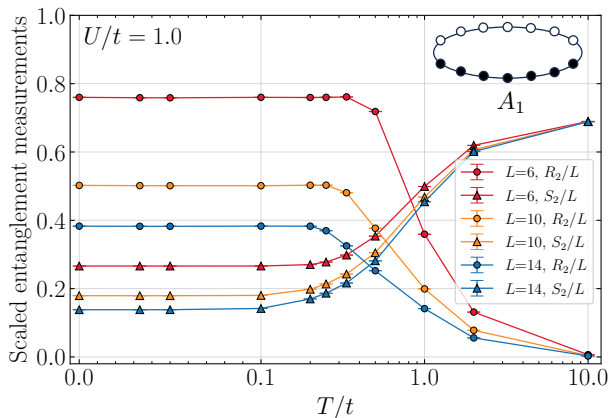


FIG. 2. Quantum-classical crossover. The scaled Rényi negativity ratio R_2/L and EE S_2/L of the half-filled Hubbard chain under a half-chain bipartition vary as functions of temperature. As the temperature rises, the scaled EE for different lengths increases and converges, indicating a dominance of volume law at high temperatures. Meanwhile, the negativity ratio begins to vanish once the temperature reaches a critical value associated with the finite-size gap $1/L$ [62].

length, the plateau becomes narrower. In summary, the monotonic decay of the negativity ratio with rising temperature signifies a crossover from a quantum entangled state to a classical mixed state.

Finite-temperature transition in t - V model.—To demonstrate the efficacy of Rényi negativity ratio in detecting finite-temperature phase transition, we further consider the half-filled spinless t - V model on a square lattice with periodic boundary conditions [82–84],

$$H = -t \sum_{\langle i,j \rangle} (c_i^\dagger c_j + c_j^\dagger c_i) + V \sum_{\langle i,j \rangle} \left(n_i - \frac{1}{2} \right) \left(n_j - \frac{1}{2} \right), \quad (10)$$

where both the hopping and the interaction involve only nearest neighbors. In the presence of a finite coupling parameter V , this model exhibits a charge density wave (CDW) ground state and undergoes a phase transition from the CDW phase to a metallic phase at finite temperature, with critical behavior falling within the 2D Ising universality class [84, 85]. In the following, we focus on a specific coupling strength, $V/t = 2$, where the critical temperature is estimated to be approximately $T_c/t \approx 1.0$, a value lower than the 2D Ising result of $0.56|V/t| = 1.12$ [84].

This model is also a sign-problem-free model [86–89]. However, for models with larger dimensions or stronger interaction strengths, the direct sampling of Rényi negativity using Eq. (8) becomes inaccurate and challenging to converge, as a result of the occurrence of spikes [90] or the non-Gaussian distribution of Grover determinants $\det g_x = \det[G_{\mathbf{s}_1}^{T_2^f} G_{\mathbf{s}_2}^{T_2^f} + (I - G_{\mathbf{s}_1}^{T_2^f})(I - G_{\mathbf{s}_2}^{T_2^f})]$ [91]. We

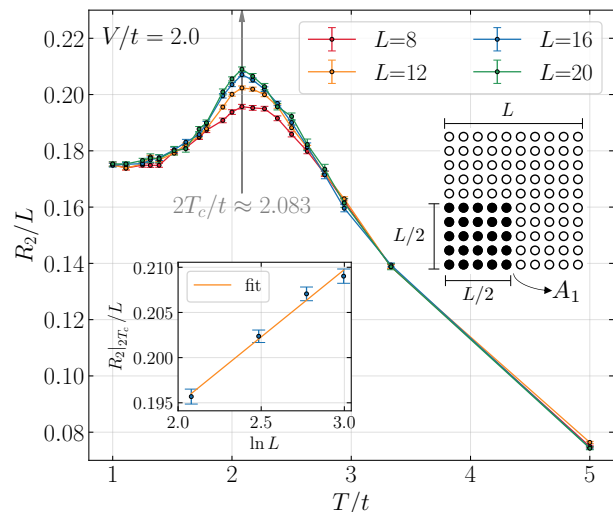


FIG. 3. The finite temperature transition in the spinless t - V model is detected by the area-law coefficient of the Rényi negativity ratio as a function of temperature. The geometry of the bipartition is illustrated in the inset on the right. A vertical arrow, colored in gray, indicates the position of the shared peak, with half of it aligning with the transition point determined in previous studies [82, 84]. The left inset shows the linear scaling of the area-law coefficient at the critical point with $\ln L$.

implement an incremental algorithm for rank- n Rényi negativity, analogous to the controllable incremental algorithm for Rényi EE [91–94], the spirit of which is to measure $(\det g_x)^{1/N_{\text{inc}}}$ instead of $(\det g_x)$ to circumvent the sampling of an exponentially small quantity with exponentially large variance [95]. It is important to note that there is a sign ambiguity in the N_{inc} -th root. In the Supplementary Material [70], we prove that the Grover determinant $\det g_x$ is always real and non-negative for two classes of sign-free models, represented by the Hubbard model and the spinless t - V model, respectively.

As illustrated in the right inset of Fig. 3, we designate the lower left corner with dimensions $(L/2) \times (L/2)$ as subsystem A_1 , resulting in an area-law coefficient of the Rényi negativity ratio of R_2/L . The main plot of Fig. 3 presents R_2/L as a function of temperature for various system sizes, demonstrating a notably distinct finite-size characteristic compared to the intersection of mutual information [82, 96–98]. Remarkably, unlike the Hubbard model in Fig. 2 or the previous study on the 2+1D transverse field Ising model [47], the Rényi negativity ratio does not exhibit a monotonic decrease with rising temperature. Instead, for varying lattice sizes, a shared local maximum appears at approximately twice the transition temperature, $2T_c/t \approx 2.1$. The inclusion of the prefactor 2 aligns with the rank of the Rényi negativity ratio under consideration, consistent with earlier discussion on

the critical behavior of Rényi negativity [47, 51, 53]. The peak of R_2/L exhibits a logarithmic divergence with system size L as shown in the left inset of Fig. 3, while the area law is well preserved far away from the critical point [99]. Based on symmetry considerations, it was argued that the entanglement negativity inherits the singularity of the specific heat at a finite temperature transition [47, 53], and for the 2D Ising transition, the specific heat has a logarithmic divergence. However, in our fermionic scenario, the quantity showing this divergence is R_2/L rather than its temperature derivative. The underlying cause of the logarithmic divergence of R_2/L at $2T_c$ thus remains an unresolved issue.

Conclusions and outlook.—We showed that the partially transposed density matrix for interacting fermions, akin to the reduced density matrix, can be expanded as a weighted sum of Gaussian states representing free fermions, thereby paving the way for the study of mixed-state entanglement in strongly correlated fermionic systems. This main result was employed to implement an algorithm to compute the rank- n Rényi negativity for interacting fermionic systems within the DQMC framework. We presented the first study of the rank-two Rényi negativity for the half-filled Hubbard chain and the spinless t - V model on a square lattice. Remarkably, we found that the area law coefficient of the negativity ratio exhibits a logarithmic singular peak at twice the finite-temperature transition point for all lattice sizes under consideration.

There are several potential future research directions to consider. The first direction is to investigate the finite-temperature entanglement of various interacting fermionic models, especially those with transition points that belong to different universality classes, such as the 3D Hubbard model which owns a transition belonging to $O(3)$ universality class [100]. Further, exploring the entanglement in other types of mixed states, such as tripartite ground states of topological [57] and gapless systems [39], and measurement-induced mixed states [101, 102] presents an intriguing avenue for further research. Next, exploring the finite-size scaling laws of negativity in interacting fermionic systems, especially the beyond-area-law behaviors that reveal universal properties of quantum systems, could also be intriguing. In particular, our finding of the $L \ln L$ scaling of the negativity ratio at the critical point in the spinless t - V model may indicate long-range entanglement contribution [47, 65], which warrants further investigation. Moreover, our results are applicable to the continuous-time QMC method, offering an opportunity to study the mixed-state entanglement of realistic correlated materials through combining with dynamical mean-field theory [82, 103, 104]. For example, to fit into the hybridization expansion algorithm, the bath can be first traced out [66, 78] and then the density matrix of the impurity can be obtained using the Green's functions and density correlation functions [65, 105]. Another interesting

example is to integrate the rank-two Rényi negativity into the interaction expansion algorithm by making use the identity $\text{Tr}[(\rho^{T_2}^2)] = \text{Tr}[(\rho X_2(\pi))^2]$, where the disorder operator, expressed in the interaction picture as $X_2(\tau) \propto \prod_{j \in A_2, \sigma} (n_{i\sigma}(\tau) - \frac{1}{2})$, is nothing just some additional interaction vertices only at A_2 subregion. Finally, another proposal for realistic materials is to integrate the Rényi negativity into the constrained-path auxiliary-field QMC method [106–109] which controls the sign problem.

Acknowledgements.—We thank Tarun Grover for helpful discussions and comments on the draft. This work is supported by the National Key R&D Program of China (Grant No. 2022YFA1402702, No. 2021YFA1401400), the National Natural Science Foundation of China (Grants No. 12274289), the Innovation Program for Quantum Science and Technology (under Grant No. 2021ZD0301902), Yangyang Development Fund, and startup funds from SJTU. The computations in this paper were run on the Siyuan-1 and π 2.0 clusters supported by the Center for High Performance Computing at Shanghai Jiao Tong University.

* xiaoyanxu@sjtu.edu.cn

- [1] G. Vidal, J. I. Latorre, E. Rico, and A. Kitaev, Entanglement in Quantum Critical Phenomena, *Physical Review Letters* **90**, 227902 (2003).
- [2] L. Amico, R. Fazio, A. Osterloh, and V. Vedral, Entanglement in many-body systems, *Reviews of Modern Physics* **80**, 517 (2008).
- [3] N. Laflorencie, Quantum entanglement in condensed matter systems, *Physics Reports* **646**, 1 (2016).
- [4] P. Calabrese, J. Cardy, and B. Doyon, Entanglement entropy in extended quantum systems, *Journal of Physics A: Mathematical and Theoretical* **42**, 500301 (2009).
- [5] M. Srednicki, Entropy and area, *Physical Review Letters* **71**, 666 (1993).
- [6] M. M. Wolf, F. Verstraete, M. B. Hastings, and J. I. Cirac, Area Laws in Quantum Systems: Mutual Information and Correlations, *Physical Review Letters* **100**, 070502 (2008).
- [7] J. Eisert, M. Cramer, and M. B. Plenio, *Colloquium*: Area laws for the entanglement entropy, *Reviews of Modern Physics* **82**, 277 (2010).
- [8] C. Holzhey, F. Larsen, and F. Wilczek, Geometric and renormalized entropy in conformal field theory, *Nuclear Physics B* **424**, 443 (1994).
- [9] P. Calabrese and J. Cardy, Entanglement entropy and quantum field theory, *Journal of Statistical Mechanics: Theory and Experiment* **2004**, P06002 (2004).
- [10] D. Gioev and I. Klich, Entanglement Entropy of Fermions in Any Dimension and the Widom Conjecture, *Physical Review Letters* **96**, 100503 (2006).
- [11] B. Swingle, Entanglement Entropy and the Fermi Surface, *Physical Review Letters* **105**, 050502 (2010).
- [12] R. V. Mishmash and O. I. Motrunich, Entanglement entropy of composite Fermi liquid states on the lattice: In support of the Widom formula, *Physical Review B*

- 94**, 081110 (2016).
- [13] E. Fradkin and J. E. Moore, Entanglement Entropy of 2D Conformal Quantum Critical Points: Hearing the Shape of a Quantum Drum, *Physical Review Letters* **97**, 050404 (2006).
- [14] H. Casini and M. Huerta, Universal terms for the entanglement entropy in 2+1 dimensions, *Nuclear Physics B* **764**, 183 (2007).
- [15] A. B. Kallin, M. B. Hastings, R. G. Melko, and R. R. P. Singh, Anomalies in the entanglement properties of the square-lattice Heisenberg model, *Physical Review B* **84**, 165134 (2011).
- [16] H. F. Song, N. Laflorencie, S. Rachel, and K. Le Hur, Entanglement entropy of the two-dimensional Heisenberg antiferromagnet, *Physical Review B* **83**, 224410 (2011).
- [17] M. A. Metlitski and T. Grover, *Entanglement Entropy of Systems with Spontaneously Broken Continuous Symmetry* (2015), arxiv:1112.5166 [cond-mat, physics:hep-th, physics:quant-ph].
- [18] Y. D. Liao, G. Pan, W. Jiang, Y. Qi, and Z. Y. Meng, The teaching from entanglement: 2D SU(2) antiferromagnet to valence bond solid deconfined quantum critical points are not conformal (2023), arxiv:2302.11742 [cond-mat, physics:math-ph, physics:physics, physics:quant-ph].
- [19] A. Kitaev and J. Preskill, Topological Entanglement Entropy, *Physical Review Letters* **96**, 110404 (2006).
- [20] M. Levin and X.-G. Wen, Detecting Topological Order in a Ground State Wave Function, *Physical Review Letters* **96**, 110405 (2006).
- [21] S. V. Isakov, M. B. Hastings, and R. G. Melko, Topological entanglement entropy of a Bose-Hubbard spin liquid, *Nature Physics* **7**, 772 (2011).
- [22] H.-C. Jiang, Z. Wang, and L. Balents, Identifying topological order by entanglement entropy, *Nature Physics* **8**, 902 (2012).
- [23] S. Sankar, E. Sela, and C. Han, Measuring Topological Entanglement Entropy Using Maxwell Relations, *Physical Review Letters* **131**, 016601 (2023).
- [24] M. B. Plenio and S. Virmani, An introduction to entanglement measures, *Quantum Information & Computation* **7**, 1 (2007).
- [25] R. Horodecki, P. Horodecki, M. Horodecki, and K. Horodecki, Quantum entanglement, *Reviews of Modern Physics* **81**, 865 (2009).
- [26] K. Życzkowski, P. Horodecki, A. Sanpera, and M. Lewenstein, Volume of the set of separable states, *Physical Review A* **58**, 883 (1998).
- [27] J. Eisert and M. B. Plenio, A comparison of entanglement measures, *Journal of Modern Optics* **46**, 145 (1999).
- [28] G. Vidal and R. F. Werner, Computable measure of entanglement, *Physical Review A* **65**, 032314 (2002).
- [29] M. B. Plenio, Logarithmic Negativity: A Full Entanglement Monotone That is not Convex, *Physical Review Letters* **95**, 090503 (2005).
- [30] A. Peres, Separability Criterion for Density Matrices, *Physical Review Letters* **77**, 1413 (1996).
- [31] M. Horodecki, P. Horodecki, and R. Horodecki, Separability of mixed states: Necessary and sufficient conditions, *Physics Letters A* **223**, 1 (1996).
- [32] P. Calabrese, J. Cardy, and E. Tonni, Entanglement Negativity in Quantum Field Theory, *Physical Review Letters* **109**, 130502 (2012).
- [33] P. Calabrese, J. Cardy, and E. Tonni, Entanglement negativity in extended systems: A field theoretical approach, *Journal of Statistical Mechanics: Theory and Experiment* **2013**, P02008 (2013).
- [34] P. Calabrese, J. Cardy, and E. Tonni, Finite temperature entanglement negativity in conformal field theory, *Journal of Physics A: Mathematical and Theoretical* **48**, 015006 (2014).
- [35] X. Wen, P.-Y. Chang, and S. Ryu, Entanglement negativity after a local quantum quench in conformal field theories, *Physical Review B* **92**, 075109 (2015).
- [36] K. Audenaert, J. Eisert, M. B. Plenio, and R. F. Werner, Entanglement properties of the harmonic chain, *Physical Review A* **66**, 042327 (2002).
- [37] C.-M. Chung, V. Alba, L. Bonnes, P. Chen, and A. M. Läuchli, Entanglement negativity via the replica trick: A quantum Monte Carlo approach, *Physical Review B* **90**, 064401 (2014).
- [38] V. Eisler and Z. Zimborás, Entanglement negativity in the harmonic chain out of equilibrium, *New Journal of Physics* **16**, 123020 (2014).
- [39] V. Eisler and Z. Zimborás, Entanglement negativity in two-dimensional free lattice models, *Physical Review B* **93**, 115148 (2016).
- [40] C. De Nobili, A. Coser, and E. Tonni, Entanglement negativity in a two dimensional harmonic lattice: Area law and corner contributions, *Journal of Statistical Mechanics: Theory and Experiment* **2016**, 083102 (2016).
- [41] H. Wichterich, J. Vidal, and S. Bose, Universality of the negativity in the Lipkin-Meshkov-Glick model, *Physical Review A* **81**, 032311 (2010).
- [42] R. A. Santos, V. Korepin, and S. Bose, Negativity for two blocks in the one-dimensional spin-1 Affleck-Kennedy-Lieb-Tasaki model, *Physical Review A* **84**, 062307 (2011).
- [43] A. Bayat, S. Bose, P. Sodano, and H. Johannesson, Entanglement Probe of Two-Impurity Kondo Physics in a Spin Chain, *Physical Review Letters* **109**, 066403 (2012).
- [44] P. Calabrese, L. Tagliacozzo, and E. Tonni, Entanglement negativity in the critical Ising chain, *Journal of Statistical Mechanics: Theory and Experiment* **2013**, P05002 (2013).
- [45] V. Alba, Entanglement negativity and conformal field theory: A Monte Carlo study, *Journal of Statistical Mechanics: Theory and Experiment* **2013**, P05013 (2013).
- [46] N. E. Sherman, T. Devakul, M. B. Hastings, and R. R. P. Singh, Nonzero-temperature entanglement negativity of quantum spin models: Area law, linked cluster expansions, and sudden death, *Physical Review E* **93**, 022128 (2016).
- [47] K.-H. Wu, T.-C. Lu, C.-M. Chung, Y.-J. Kao, and T. Grover, Entanglement Renyi Negativity across a Finite Temperature Transition: A Monte Carlo study, *Physical Review Letters* **125**, 140603 (2020).
- [48] C. Castelnuovo, Negativity and topological order in the toric code, *Physical Review A* **88**, 042319 (2013).
- [49] Y. A. Lee and G. Vidal, Entanglement negativity and topological order, *Physical Review A* **88**, 042318 (2013).
- [50] O. Hart and C. Castelnuovo, Entanglement negativity and sudden death in the toric code at finite temperature, *Physical Review B* **97**, 144410 (2018).

- [51] T.-C. Lu and T. Grover, Singularity in entanglement negativity across finite-temperature phase transitions, *Physical Review B* **99**, 075157 (2019).
- [52] T.-C. Lu, T. H. Hsieh, and T. Grover, Detecting topological order at finite temperature using entanglement negativity, *Physical Review Letters* **125**, 116801 (2020).
- [53] T.-C. Lu and T. Grover, Structure of quantum entanglement at a finite temperature critical point, *Physical Research* **2**, 043345 (2020).
- [54] V. Eisler and Z. Zimborás, On the partial transpose of fermionic Gaussian states, *New Journal of Physics* **17**, 053048 (2015).
- [55] J. Eisert, V. Eisler, and Z. Zimborás, Entanglement negativity bounds for fermionic Gaussian states, *Physical Review B* **97**, 165123 (2018).
- [56] H. Shapourian, K. Shiozaki, and S. Ryu, Partial time-reversal transformation and entanglement negativity in fermionic systems, *Physical Review B* **95**, 165101 (2017).
- [57] K. Shiozaki, H. Shapourian, K. Gomi, and S. Ryu, Many-body topological invariants for fermionic short-range entangled topological phases protected by antiunitary symmetries, *Physical Review B* **98**, 035151 (2018).
- [58] H. Shapourian and S. Ryu, Entanglement negativity of fermions: Monotonicity, separability criterion, and classification of few-mode states, *Physical Review A* **99**, 022310 (2019).
- [59] P.-Y. Chang and X. Wen, Entanglement negativity in free-fermion systems: An overlap matrix approach, *Physical Review B* **93**, 195140 (2016).
- [60] A. Coser, E. Tonni, and P. Calabrese, Towards the entanglement negativity of two disjoint intervals for a one dimensional free fermion, *Journal of Statistical Mechanics: Theory and Experiment* **2016**, 033116 (2016).
- [61] C. P. Herzog and Y. Wang, Estimation for entanglement negativity of free fermions, *Journal of Statistical Mechanics: Theory and Experiment* **2016**, 073102 (2016).
- [62] H. Shapourian and S. Ryu, Finite-temperature entanglement negativity of free fermions, *Journal of Statistical Mechanics: Theory and Experiment* **2019**, 043106 (2019).
- [63] V. Alba and F. Carollo, Logarithmic negativity in out-of-equilibrium open free-fermion chains: An exactly solvable case, *SciPost Physics* **15**, 124 (2023), [arxiv:2205.02139](https://arxiv.org/abs/2205.02139) [cond-mat, physics:hep-th, physics:quant-ph].
- [64] W. Choi, M. Knap, and F. Pollmann, *Finite Temperature Entanglement Negativity of Fermionic Symmetry Protected Topological Phases and Quantum Critical Points in One Dimension* (2023), [arxiv:2310.20566](https://arxiv.org/abs/2310.20566) [cond-mat].
- [65] G. Perez and W. Witczak-Krempa, *Are fermionic quantum critical systems more entangled?* (2023), [arxiv:2310.15273](https://arxiv.org/abs/2310.15273) [cond-mat.str-el].
- [66] T. Grover, Entanglement of Interacting Fermions in Quantum Monte Carlo Calculations, *Physical Review Letters* **111**, 130402 (2013).
- [67] R. Blankenbecler, D. J. Scalapino, and R. L. Sugar, Monte Carlo calculations of coupled boson-fermion systems. I, *Physical Review D* **24**, 2278 (1981).
- [68] D. J. Scalapino and R. L. Sugar, Monte Carlo calculations of coupled boson-fermion systems. II, *Physical Review B* **24**, 4295 (1981).
- [69] F. Assaad and H. Evertz, World-line and Determinantal Quantum Monte Carlo Methods for Spins, Phonons and Electrons, in *Computational Many-Particle Physics*, Lecture Notes in Physics, edited by H. Fehske, R. Schneider, and A. Weiße (Springer, Berlin, Heidelberg, 2008) pp. 277–356.
- [70] See the Supplemental Material, which additionally includes Refs. [71–76], for (i) a review of fermionic partial transpose, (ii) a brief introduction to determinant quantum Monte Carlo, (iii) details of DQMC implement of Rényi negativity, (iv) additional plots of the Rényi negativity, and (v) the proof of sign-free Grover determinants in Hubbard model and t - V model.
- [71] E. Fradkin, Disorder Operators and Their Descendants, *Journal of Statistical Physics* **167**, 427 (2017).
- [72] Z. H. Liu, Y. D. Liao, G. Pan, M. Song, J. Zhao, W. Jiang, C.-M. Jian, Y.-Z. You, F. F. Assaad, Z. Y. Meng, and C. Xu, Disorder Operator and Rényi Entanglement Entropy of Symmetric Mass Generation, *Physical Review Letters* **132**, 156503 (2024).
- [73] F. Sun and X. Y. Xu, *Delay Update in Determinant Quantum Monte Carlo* (2023), [arxiv:2308.12005](https://arxiv.org/abs/2308.12005) [cond-mat].
- [74] G. H. Lang, C. W. Johnson, S. E. Koonin, and W. E. Ormand, Monte Carlo evaluation of path integrals for the nuclear shell model, *Physical Review C* **48**, 1518 (1993).
- [75] I. Klich, A note on the full counting statistics of paired fermions, *Journal of Statistical Mechanics: Theory and Experiment* **2014**, P11006 (2014).
- [76] Z.-C. Wei, *Semigroup Approach to the Sign Problem in Quantum Monte Carlo Simulations* (2018), [arxiv:1712.09412](https://arxiv.org/abs/1712.09412) [cond-mat, physics:hep-lat, physics:math-ph, physics:nucl-th].
- [77] The proof uses the Wick theorem for Majorana monomial, see Ref. [54] and Supplementary Material (SM) [70] for details.
- [78] S.-A. Cheong and C. L. Henley, Many-body density matrices for free fermions, *Physical Review B* **69**, 075111 (2004).
- [79] We utilized the definition of fermionic partial transpose in Fock space for exact diagonalization, see the formula Eqs. (S2) and (S3) in SM [70].
- [80] We note that in the context of studying fermionic systems, an alternative definition for the moments of the PTDM is given by $\text{Tr}(\rho^{T_2^f} \rho^{T_2^{f\dagger}} \dots)$ [56, 62, 65], which aims to account for the non-Hermitian nature and potential complex eigenvalues associated with the partial time reversal of the density matrix. However, the models under consideration in this letter do not exhibit this issue due to specific symmetries they possess that circumvent the sign problem.
- [81] P. Broecker and S. Trebst, Rényi entropies of interacting fermions from determinantal quantum Monte Carlo simulations, *Journal of Statistical Mechanics: Theory and Experiment* **2014**, P08015 (2014).
- [82] L. Wang and M. Troyer, Rényi Entanglement Entropy of Interacting Fermions Calculated Using the Continuous-Time Quantum Monte Carlo Method, *Physical Review Letters* **113**, 110401 (2014).
- [83] D. J. Scalapino, R. L. Sugar, and W. D. Toussaint, Monte Carlo study of a two-dimensional spin-polarized fermion lattice gas, *Physical Review B* **29**, 5253 (1984).
- [84] J. E. Gubernatis, D. J. Scalapino, R. L. Sugar,

- and W. D. Toussaint, Two-dimensional spin-polarized fermion lattice gases, *Physical Review B* **32**, 103 (1985).
- [85] S. Hesselmann and S. Wessel, Thermal Ising transitions in the vicinity of two-dimensional quantum critical points, *Physical Review B* **93**, 155157 (2016).
- [86] E. F. Huffman and S. Chandrasekharan, Solution to sign problems in half-filled spin-polarized electronic systems, *Physical Review B* **89**, 111101 (2014).
- [87] Z.-X. Li, Y.-F. Jiang, and H. Yao, Solving the fermion sign problem in quantum Monte Carlo simulations by Majorana representation, *Physical Review B* **91**, 241117 (2015).
- [88] L. Wang, Y.-H. Liu, M. Iazzi, M. Troyer, and G. Harcos, Split Orthogonal Group: A Guiding Principle for Sign-Problem-Free Fermionic Simulations, *Physical Review Letters* **115**, 250601 (2015).
- [89] Z. C. Wei, C. Wu, Y. Li, S. Zhang, and T. Xiang, Majorana Positivity and the Fermion Sign Problem of Quantum Monte Carlo Simulations, *Physical Review Letters* **116**, 250601 (2016).
- [90] H. Shi and S. Zhang, Infinite variance in fermion quantum Monte Carlo calculations, *Physical Review E* **93**, 033303 (2016).
- [91] Y. D. Liao, [Controllable Incremental Algorithm for Entanglement Entropy in Quantum Monte Carlo Simulations](#) (2023), [arxiv:2307.10602](#) [cond-mat].
- [92] J. D’Emidio, R. Orus, N. Laflorencie, and F. de Juan, [Universal features of entanglement entropy in the honeycomb Hubbard model](#) (2022), [arxiv:2211.04334](#) [cond-mat, physics:quant-ph].
- [93] G. Pan, Y. Da Liao, W. Jiang, J. D’Emidio, Y. Qi, and Z. Y. Meng, Stable computation of entanglement entropy for 2D interacting fermion systems, *Physical Review B* **108**, L081123 (2023).
- [94] X. Zhang, G. Pan, B.-B. Chen, K. Sun, and Z. Y. Meng, [An integral algorithm of exponential observables for interacting fermions in quantum Monte Carlo simulation](#) (2023), [arxiv:2311.03448](#) [cond-mat, physics:quant-ph].
- [95] In preparation.
- [96] R. G. Melko, A. B. Kallin, and M. B. Hastings, Finite-size scaling of mutual information in Monte Carlo simulations: Application to the spin- $\frac{1}{2}$ XXZ model, *Physical Review B* **82**, 100409 (2010).
- [97] R. R. P. Singh, M. B. Hastings, A. B. Kallin, and R. G. Melko, Finite-Temperature Critical Behavior of Mutual Information, *Physical Review Letters* **106**, 135701 (2011).
- [98] J. Iaconis, S. Inglis, A. B. Kallin, and R. G. Melko, Detecting classical phase transitions with Renyi mutual information, *Physical Review B* **87**, 195134 (2013).
- [99] This beyond-area-law scaling around the finite temperature critical point is also observed for other values of V , a different bipartite geometry, and a different lattice. Refer to the SM for additional complementary plots [70].
- [100] H. Yanatori and A. Koga, Finite-temperature phase transitions in the $SU(N)$ Hubbard model, *Physical Review B* **94**, 041110 (2016).
- [101] G.-Y. Zhu and S. Trebst, [Qubit fractionalization and emergent Majorana liquid in the honeycomb Floquet code induced by coherent errors and weak measurements](#) (2023), [arxiv:2311.08450](#) [cond-mat, physics:quant-ph].
- [102] Y.-H. Chen and T. Grover, [Symmetry-enforced many-body separability transitions](#) (2023), [arxiv:2310.07286](#) [cond-mat, physics:hep-th, physics:quant-ph].
- [103] E. Gull, A. J. Millis, A. I. Lichtenstein, A. N. Rubtsov, M. Troyer, and P. Werner, Continuous-time Monte Carlo methods for quantum impurity models, *Reviews of Modern Physics* **83**, 349 (2011).
- [104] A. Georges, G. Kotliar, W. Krauth, and M. J. Rozenberg, Dynamical mean-field theory of strongly correlated fermion systems and the limit of infinite dimensions, *Reviews of Modern Physics* **68**, 13 (1996).
- [105] T.-T. Wang, M. Song, L. Lyu, W. Witczak-Krempa, and Z. Y. Meng, [Entanglement Microscopy: Tomography and Entanglement Measures via Quantum Monte Carlo](#) (2024), [arxiv:2402.14916](#) [cond-mat, physics:hep-th, physics:quant-ph].
- [106] S. Zhang, J. Carlson, and J. E. Gubernatis, Constrained Path Quantum Monte Carlo Method for Fermion Ground States, *Physical Review Letters* **74**, 3652 (1995).
- [107] S. Zhang, J. Carlson, and J. E. Gubernatis, Constrained path Monte Carlo method for fermion ground states, *Physical Review B* **55**, 7464 (1997).
- [108] S. Zhang, Finite-Temperature Monte Carlo Calculations for Systems with Fermions, *Physical Review Letters* **83**, 2777 (1999).
- [109] Y.-Y. He, M. Qin, H. Shi, Z.-Y. Lu, and S. Zhang, Finite-temperature auxiliary-field quantum Monte Carlo: Self-consistent constraint and systematic approach to low temperatures, *Physical Review B* **99**, 045108 (2019).

The Supplementary Material for “Entanglement Rényi negativity of interacting fermions from quantum Monte Carlo simulations”

Fo-Hong Wang¹ and Xiao Yan Xu^{1,2,*}

¹Key Laboratory of Artificial Structures and Quantum Control (Ministry of Education),
School of Physics and Astronomy, Shanghai Jiao Tong University, Shanghai 200240, China
²Hefei National Laboratory, University of Science and Technology of China, Hefei 230088, China
(Dated: April 30, 2024)

CONTENTS

Fermionic partial transpose in different representations	0
Determinant Quantum Monte Carlo Methods	1
Finite-temperature Scheme	1
Zero-temperature Projector Scheme	2
Other details of the DQMC simulations	3
DQMC implementation of fermionic partial transpose	3
Additional results of the Rényi negativity	5
Sign problem of Grover determinant	6
Sufficient Condition I: $G_{ij}^\dagger = (-)^{i+j}(\delta_{ij} - G_{ji}^{\dagger*})$	7
Sufficient Condition II: $\Gamma_{ij}^{(2)} = (-)^{i+j}\Gamma_{ij}^{(1)*}$	8
References	8

FERMIONIC PARTIAL TRANSPOSE IN DIFFERENT REPRESENTATIONS

In this section, we briefly review the definition of fermionic partial transpose, which does not follow the original definition [S1] extensively used in bosonic systems. Consider a lattice model described by complex fermion operators c_j and c_j^\dagger satisfying anticommutation relations $\{c_j, c_k^\dagger\} = \delta_{jk}$, where $j, k = 1, \dots, N$ are labels of sites (for simplicity we omit the index for internal degree of freedom). For convenience, we also introduce the Majorana basis, denoted as $\gamma_{2j-1} = c_j + c_j^\dagger$ and $\gamma_{2j} = -i(c_j - c_j^\dagger)$. Under a bipartite scheme that divides the total system as $A = A_1 \cup A_2$, the fermionic partial transpose with respect to subsystem A_2 , denoted by $\mathcal{O}^{T_2^f}$ with \mathcal{O} as an operator (like the density operator ρ or just a single basis operator $|e_j\rangle\langle\bar{e}_j|$), is first defined in the coherent basis as [S2]

$$U_{A_2} (|\{\xi_j\}_{j \in A_1}, \{\xi_j\}_{j \in A_2}\rangle\langle\{\bar{\chi}_j\}_{j \in A_1}, \{\bar{\chi}_j\}_{j \in A_2}|)^{T_2^f} U_{A_2}^\dagger = |\{\xi_j\}_{j \in A_1}, \{-i\bar{\chi}_j\}_{j \in A_2}\rangle\langle\{\bar{\chi}_j\}_{j \in A_1}, \{-i\xi_j\}_{j \in A_2}|, \quad (\text{S1})$$

where $|\{\xi_j\}\rangle = e^{-\sum_j \xi_j c_j^\dagger} |0\rangle$ and $\langle\{\bar{\chi}_j}\rangle = \langle 0| e^{-\sum_j c_j \bar{\chi}_j}$ are the fermion coherent states, and $U_{A_2} \equiv \prod_{j \in A_2} \gamma_{2j-1}$ is the partial particle-hole transformation which only turns the particles (holes) in the subsystem A_2 into holes (particles). After choosing an appropriate ordering such that $A_2 = \{N_1 + 1, \dots, N\}$, one obtains fermionic partial transpose in the occupation number basis by expressing the coherent states in Eq. (S1) in terms of Fock states [S2, S3]

$$(|\{n_j\}_{j \in A_1}, \{n_j\}_{j \in A_2}\rangle\langle\{\bar{n}_j\}_{j \in A_1}, \{\bar{n}_j\}_{j \in A_2}|)^{T_2^f} = (-1)^{\phi(\{n_j\}, \{\bar{n}_j\})} |\{n_j\}_{j \in A_1}, \{\bar{n}_j\}_{j \in A_2}\rangle\langle\{\bar{n}_j\}_{j \in A_1}, \{n_j\}_{j \in A_2}|, \quad (\text{S2})$$

which is similar to the conventional partial transpose up to an additional phase factor

$$\phi(\{n_j\}, \{\bar{n}_j\}) = [(\tau_2 + \bar{\tau}_2) \bmod 2] / 2 + (\tau_1 + \bar{\tau}_1)(\tau_2 + \bar{\tau}_2) \quad (\text{S3})$$

with $\tau_b = \sum_{j \in A_b} n_j$ the number of particles in subsystem A_b ($b = 1, 2$). The definition in Eq. (S2) has been employed in the exact diagonalization calculations in Fig. 1 of the main text. Moreover, utilizing this definition, it is straightforward to show that

$$\begin{aligned} \text{Tr} \left[(\rho^{T_2^f})^k \right] &= \sum_{\{n_j^{(1)}\} \dots \{n_j^{(k)}\}} \langle \{n_j^{(1)}\} | \rho | \{n_j^{(2)}\} \rangle \langle \{n_j^{(2)}\} | \rho | \{n_j^{(3)}\} \rangle \dots \langle \{n_j^{(i)}\} | \rho | \{n_j^{(i+1)}\} \rangle \dots \langle \{n_j^{(k)}\} | \rho | \{n_j^{(1)}\} \rangle \\ &\times (-1)^{\phi(\{n_j^{(1)}\}, \{n_j^{(2)}\})} (-1)^{\phi(\{n_j^{(2)}\}, \{n_j^{(3)}\})} \dots (-1)^{\phi(\{n_j^{(i)}\}, \{n_j^{(i+1)}\})} \dots (-1)^{\phi(\{n_j^{(k)}\}, \{n_j^{(1)}\})}. \end{aligned} \quad (\text{S4})$$

Specifically, note that $(-1)^{\phi(\{n_j\}, \{n_j\})} = 1$ and $\phi(\{n_j\}, \{\bar{n}_j\}) = \phi(\{\bar{n}_j\}, \{n_j\})$, one can deduce that $\text{Tr}[\rho^{T_2^f}] = \text{Tr}[\rho] = 1$ while $\text{Tr}[(\rho^{T_2^f})^2] = \text{Tr}[(\rho \hat{X}_2(\pi))^2]$ with $\hat{X}_2(\theta) = e^{i\theta \sum_{j \in A_2} \hat{n}_j}$ being the disorder operator and $\hat{n}_j = c_j^\dagger c_j$ the local density operator [S4, S5].

In general, density operators can be written as a restricted superposition of products of Majorana operators. Assume that there are k (l) sites in subsystem A_1 (A_2), in which the Majorana indices are denoted by $\{m_1, \dots, m_{2k}\}$ ($\{n_1, \dots, n_{2l}\}$), a density operator can be expressed as [S6, S7]

$$\rho = \sum_{\substack{\kappa, \tau, \\ |\kappa| + |\tau| = \text{even}}} w_{\kappa, \tau} \gamma_{m_1}^{\kappa_1} \dots \gamma_{m_{2k}}^{\kappa_{2k}} \gamma_{n_1}^{\tau_1} \dots \gamma_{n_{2l}}^{\tau_{2l}} \quad (\text{S5})$$

where $\kappa = (\kappa_1, \dots, \kappa_{2k})$ and $\tau = (\tau_1, \dots, \tau_{2l})$ represent various Majorana configurations. Here, κ_i and τ_j are the occupations of single Majorana modes, and $|\kappa| = \sum_j \kappa_j$ or $|\tau| = \sum_j \tau_j$ is the total number of Majorana fermions in the corresponding subsystem. We note that $w_{\kappa, \tau} \neq 0$ only if $|\kappa| + |\tau|$ is even since a physical state must have a specific parity. Now, we evaluate the fermionic partial transpose $\rho^{T_2^f}$ based on Eq. (S5), and for each term, the operators in subsystem A_2 would be transformed to $\mathcal{R}_2^f(\gamma_{n_1}^{\tau_1} \dots \gamma_{n_{2l}}^{\tau_{2l}})$. It turns out that the definition in Eq. (S1) would give us a simple expression for the transformation \mathcal{R}_2^f [S7],

$$\mathcal{R}_2^f(\gamma_j) = i\gamma_j, \quad j \in A_2. \quad (\text{S6})$$

Under this fermionic partial transpose, a Gaussian state $\rho_0 = \det[1 + e^W]^{-1/2} \exp\left(\frac{1}{4} \sum_{k, l} W_{kl} \gamma_k \gamma_l\right)$ will be transformed to another Gaussian state.

DETERMINANT QUANTUM MONTE CARLO METHODS

In this section, we provide a brief introduction to determinant quantum Monte Carlo (DQMC) methods [S8]. For our purpose, both the zero-temperature projector scheme and the finite-temperature scheme have been used in the main text.

Finite-temperature Scheme

At a finite temperature T , and assuming that the system of interest is in thermodynamic equilibrium, we can analyze it within the framework of the grand canonical ensemble, using the partition function $Z = \text{Tr} [e^{-\beta H}]$. A generic Hamiltonian H consists of a free-particle term and an interaction term, denoted as $H = H_0 + H_I$. To compute the trace over Fock space, we employ Trotter decomposition and Hubbard-Stratonovich (HS) transformation to factorize the exponential operator $e^{-\beta H}$ into a sum of products of Gaussian operators,

$$\begin{aligned} Z &= \text{Tr} [e^{-\beta H}] = \text{Tr} \left[(e^{-\Delta_\tau H})^{L_\tau} \right] \\ &= \text{Tr} [e^{-\Delta_\tau H_0} e^{-\Delta_\tau H_U} \dots e^{-\Delta_\tau H_0} e^{-\Delta_\tau H_U}] + O(\Delta_\tau^2) \\ &\approx \sum_{\{s_{i,l}\}} \text{Tr} \left[\prod_{l=1}^{L_\tau} \left(e^{\mathbf{c}^\dagger V(l) \mathbf{c}} e^{\mathbf{c}^\dagger K \mathbf{c}} \right) \right], \end{aligned} \quad (\text{S9})$$

where $L_\tau = \beta/\Delta_\tau$ is the number of time slices, $-\Delta_\tau H_0 = \mathbf{c}^\dagger K \mathbf{c}$ with $\mathbf{c} = (c_1, \dots, c_N)^T$, and we have decoupled the interaction term H_I to fermion bilinears $\mathbf{c}^\dagger V(l) \mathbf{c} = \mathbf{c}^\dagger V[\mathbf{s}(l)] \mathbf{c}$ coupled with spacetime-dependent auxiliary fields

$\mathbf{s} = \{s_{i,l}, i \in 1, \dots, N_c; l = 1, \dots, L_\tau\}$. Here, $\mathbf{s}(l)$ includes all the auxiliary fields at time slice l and N_c represents the number of coupling terms, which varies depending on the specific interactions and decoupled channels. For the Hubbard model, we decouple it to the density channel,

$$e^{-\Delta\tau \frac{U}{2} \sum_i (n_i - 1)^2} = \sum_{\{s_i = \pm 1, \pm 2\}} \left(\prod_i \gamma(s_i) e^{-i\sqrt{\Delta\tau U/2} \eta(s_i)} \right) e^{i\sqrt{\Delta\tau U/2} \sum_i \eta(s_i) n_i}, \quad (\text{S8})$$

where $\gamma(\pm 1) = 1 + \sqrt{6}/3$, $\gamma(\pm 2) = 1 - \sqrt{6}/3$, $\eta(\pm 1) = \pm\sqrt{2(3 - \sqrt{6})}$ and $\eta(\pm 2) = \pm\sqrt{2(3 + \sqrt{6})}$. Thus, for the Hubbard model, N_c is the number of sites N . For the spinless t - V model, we decouple it to the Majorana hopping channel [S9],

$$\begin{aligned} e^{-\Delta\tau V \sum_{\langle jk \rangle} (n_i - \frac{1}{2})(n_j - \frac{1}{2})} &= \sum_{\{s_{jk} = \pm 1\}} \left(\frac{1}{2} e^{-\frac{V\Delta\tau}{4}} \right) e^{\frac{1}{2}\lambda \sum_{\langle jk \rangle} s_{jk} (i\gamma_{2i-1}\gamma_{2j-1} + i\gamma_{2i}\gamma_{2j})} \\ &= \sum_{\{s_{jk} = \pm 1\}} \left(\frac{1}{2} e^{-\frac{V\Delta\tau}{4}} \right) e^{i\lambda \sum_{\langle jk \rangle} s_{jk} (c_j^\dagger c_k - c_k^\dagger c_j)}, \end{aligned} \quad (\text{S9})$$

where $\cosh \lambda = e^{\frac{V\Delta\tau}{2}}$. Thus, for the t - V model, the subscript i of auxiliary fields $s_{i,l}$ denotes various nearest neighboring (NN) bonds $\langle jk \rangle$, and N_c represents the number of NN bonds (specifically, for bipartite lattices $N_c = Nz/2$ with z being the coordination number). The trace of products of Gaussian operators over the fermionic Fock space in the last line of Eq. (S7) can be expressed as a determinant,

$$Z = \sum_{\mathbf{s}} \omega_{\mathbf{s}} = \sum_{\mathbf{s}} \det \left[I + \prod_{l=L_\tau, \dots, 1} B(l) \right] \text{ with } B(l) = e^{V(l)} e^K. \quad (\text{S10})$$

In addition, the expectation of arbitrary operator O can also be decomposed into a sum over auxiliary fields,

$$\langle O \rangle = \frac{\text{Tr} [e^{-\beta H} O]}{\text{Tr} [e^{-\beta H}]} = \sum_{\mathbf{s}} P_{\mathbf{s}} \langle O \rangle_{\mathbf{s}} + O(\Delta\tau^2) \text{ with } P_{\mathbf{s}} = \frac{\omega_{\mathbf{s}}}{\sum_{\mathbf{s}} \omega_{\mathbf{s}}}. \quad (\text{S11})$$

Here, the expectation of O with respect to a specific configuration of auxiliary field is given by

$$\langle O \rangle_{\mathbf{s}} = \frac{\text{Tr} [U_{\mathbf{s}}(\beta, \tau) O U_{\mathbf{s}}(\tau, 0)]}{\text{Tr} U_{\mathbf{s}}(\beta, 0)} \text{ with } U_{\mathbf{s}}(\tau_2 = l_2 \Delta\tau, \tau_1 = l_1 \Delta\tau) = \prod_{l=l_1+1}^{l_2} \left(e^{\mathbf{c}^\dagger V(l) \mathbf{c}} e^{\mathbf{c}^\dagger K \mathbf{c}} \right). \quad (\text{S12})$$

For instance, the most elementary observable, namely the equal-time Green's function, can be calculated via $G_{\mathbf{s},ij}(\tau, \tau) = \langle c_i c_j^\dagger \rangle_{\mathbf{s}} = (1 + B_{\mathbf{s}}(\tau, 0) B_{\mathbf{s}}(\beta, \tau))_{ij}^{-1}$ where $B_{\mathbf{s}}(\tau_2 = l_2 \Delta\tau, \tau_1 = l_1 \Delta\tau) = \prod_{l=l_1+1}^{l_2} (e^{V(l)} e^K)$ is the matrix correspondence of $U_{\mathbf{s}}(\tau_2, \tau_1)$.

Zero-temperature Projector Scheme

In the projector DQMC scheme, the ground-state wavefunction of interest is calculated by projecting from a trial wavefunction $|\Psi_T\rangle$. It is important to note that the trial wavefunction should not be orthogonal to the true ground state $|\psi_0\rangle$ so that it is possible to obtain $|\psi_0\rangle = \lim_{\Theta \rightarrow \infty} e^{-\Theta H} |\Psi_T\rangle$ for a sufficiently long projection length Θ . Analogous to the finite temperature case, the modulus of the ground state (which plays the role of the ‘‘partition function’’) and the ground-state expectation of some observable O are written as summations over auxiliary fields after doing Trotter decomposition and HS transformation. The magnitude of the ground state is given by

$$Z = \langle \Psi_0 | \Psi_0 \rangle = \langle \Psi_T | e^{-2\Theta H} | \Psi_T \rangle \approx \sum_{\mathbf{s}} \omega_{\mathbf{s}} = \sum_{\mathbf{s}} \det [P^\dagger B_{\mathbf{s}}(2\Theta, 0) P] \quad (\text{S13})$$

where P is the coefficient matrix of the trial state determined by $|\Psi_T\rangle = \prod_{n=1}^{N_p} (\mathbf{c}^\dagger P)_n |0\rangle$, with N_p representing the number of occupied single-particle states. Here one can also see that 2Θ plays a similar role to β in the finite-temperature case. The observable expectation is given by

$$\langle O \rangle = \sum_{\mathbf{s}} P_{\mathbf{s}} \langle O \rangle_{\mathbf{s}} = \frac{\sum_{\mathbf{s}} \omega_{\mathbf{s}} \langle O \rangle_{\mathbf{s}}}{\sum_{\mathbf{s}} \omega_{\mathbf{s}}} \text{ with } \langle O \rangle_{\mathbf{s}} = \frac{\langle \Psi_T | U_{\mathbf{s}}(2\Theta, \tau) O U_{\mathbf{s}}(\tau, 0) | \Psi_T \rangle}{\langle \Psi_T | e^{-2\Theta H} | \Psi_T \rangle}. \quad (\text{S14})$$

For instance, the equal-time Green's function can be calculated as $G_{\mathbf{s}}(\tau, \tau) = I - R(\tau)(L(\tau)R(\tau))^{-1}L(\tau)$ with $R(\tau) = B_{\mathbf{s}}(\tau, 0)P$, and $L(\tau) = P^\dagger B_{\mathbf{s}}(2\Theta, \tau)$. We note that to obtain an accurate representation of the true ground state, it is advisable to only perform measurements around $\tau = \Theta$.

Other details of the DQMC simulations

The projective DQMC calculations performed in Figs. 1 and 2 of the main text used a projection length $\Theta/t = 20$, which is long enough to project the trial state to the ground state and ensures desired convergence. We chose the time slice step Δ_τ to be between 0.02 and 0.05, depending on the size of Θ or β , and the results do not change if we choose a smaller Δ_τ . The results shown in Figs. 1 and 2 of the main text were calculated without utilizing the incremental algorithm and were accelerated by employing the delay update algorithm [S10]. On the other hand, the results shown in Fig. 3 were calculated using the incremental algorithm [S11, S12], where the number of intermediate processes is 64.

DQMC IMPLEMENTATION OF FERMIONIC PARTIAL TRANSPOSE

In this section, we provide a comprehensive discussion of the DQMC implementation of fermionic partial transpose. For completeness, we begin with the formulation of DQMC in the Majorana basis and then transition back to the complex fermion basis. In the framework of DQMC, the partition function is given by $Z = \sum_{\mathbf{s}} \text{Tr} [\prod_{l=1}^{L_\tau} e^{\mathbf{c}^\dagger K_l[\mathbf{s}] \mathbf{c}}]$, where K_l combines the K and $V(l)$ in Eq. (S7), which is valid for the models being studied. We then convert to the Majorana basis by rewriting the decoupled Hamiltonian as $\mathbf{c}^\dagger K_l[\mathbf{s}] \mathbf{c} = \boldsymbol{\gamma}^T h_l[\mathbf{s}] \boldsymbol{\gamma} / 4$, where h_l is a $2N \times 2N$ antisymmetric matrix satisfying the antisymmetric condition $h_l = -h_l^T$ and $\boldsymbol{\gamma} = (\gamma_1, \dots, \gamma_{2N})$. It is worth noting that this form can encompass terms beyond particle-number conserving terms, such as pairing terms and even non-Hermitian terms [S13–S15]. The partition function in the Majorana basis is given by [S9, S14, S15]

$$\begin{aligned} Z &= \sum_{\mathbf{s}} \text{Tr} \left[e^{\frac{1}{4} \boldsymbol{\gamma}^T h_{L_\tau}[\mathbf{s}] \boldsymbol{\gamma}} \dots e^{\frac{1}{4} \boldsymbol{\gamma}^T h_l[\mathbf{s}] \boldsymbol{\gamma}} \dots e^{\frac{1}{4} \boldsymbol{\gamma}^T h_1[\mathbf{s}] \boldsymbol{\gamma}} \right] \\ &= \sum_{\mathbf{s}} \det \left[I + e^{h_{L_\tau}} \dots e^{h_l} \dots e^{h_1} \right]^{1/2}. \end{aligned} \quad (\text{S15})$$

The Green's function in this basis is defined as $\Gamma_{\mathbf{s}, kl} = \langle [\gamma_k, \gamma_l] \rangle_{\mathbf{s}} / 2 = \langle \frac{1}{4} \boldsymbol{\gamma}^T O^{kl} \boldsymbol{\gamma} \rangle_{\mathbf{s}}$ with matrix $O_{ij}^{kl} = 2\delta_{ik}\delta_{jl} - 2\delta_{il}\delta_{jk}$. Γ is also called covariance matrix which characterizes a Gaussian state with relation $\tanh(-W/2) = \Gamma$ [S6] or inverse relation $W = \ln [(I + \Gamma)^{-1}(I - \Gamma)]$. To prove these relations, we first treat O^{kl} as a generic observable and express covariance matrix Γ using propagators as in regular DQMC formulation

$$\begin{aligned} \Gamma_{\mathbf{s}, kl} &= \left\langle \frac{1}{4} \boldsymbol{\gamma}^T O^{kl} \boldsymbol{\gamma} \right\rangle_{\mathbf{s}} \\ &= \frac{\partial}{\partial \eta} \ln \text{Tr} \left[e^{\frac{1}{4} \boldsymbol{\gamma}^T h_{L_\tau}[\mathbf{s}] \boldsymbol{\gamma}} \dots e^{\frac{1}{4} \boldsymbol{\gamma}^T h_{l+1}[\mathbf{s}] \boldsymbol{\gamma}} e^{\frac{1}{4} \boldsymbol{\gamma}^T O^{kl} \boldsymbol{\gamma}} e^{\frac{1}{4} \boldsymbol{\gamma}^T h_l[\mathbf{s}] \boldsymbol{\gamma}} \dots e^{\frac{1}{4} \boldsymbol{\gamma}^T h_1[\mathbf{s}] \boldsymbol{\gamma}} \right] \Bigg|_{\eta=0} \\ &= \frac{1}{2} \frac{\partial}{\partial \eta} \text{Tr} \ln \left[I + e^{h_{L_\tau}} \dots e^{h_{l+1}} e^{\eta O^{kl}} e^{h_l} \dots e^{h_1} \right] \Bigg|_{\eta=0} = \frac{1}{2} \text{Tr} \left[A_{\mathbf{s}}(\tau, 0) (I + A_{\mathbf{s}}(\beta, 0))^{-1} A_{\mathbf{s}}(\beta, \tau) O^{kl} \right] \\ &= \frac{1}{2} \text{Tr} \left[(I - (I + A_{\mathbf{s}}(\tau, 0) A_{\mathbf{s}}(\beta, \tau))^{-1}) O^{kl} \right] = F_{kl} - F_{lk}, \end{aligned} \quad (\text{S16})$$

where $A_{\mathbf{s}}(\tau_2 = l_2 \Delta_\tau, \tau_1 = l_1 \Delta_\tau) = \prod_{l_1+1}^{l_2} e^{h_l}$ and $F(\tau, \tau) \equiv (I + A_{\mathbf{s}}(\tau, 0) A_{\mathbf{s}}(\beta, \tau))^{-1}$ are the propagators and equal-time Green's function in Majorana basis, analogous to $B_{\mathbf{s}}(\tau_2, \tau_1)$ and $G(\tau, \tau)$ defined in the last section, respectively. On the other hand, covariance matrix Γ can be evaluated using the decomposition formula of density matrix [S16]

$$\rho = \sum_{\mathbf{s}} p_{\mathbf{s}} \rho_{\mathbf{s}}, \quad \rho_{\mathbf{s}} = \det \left[I + e_{\mathbf{s}}^W \right]^{-1/2} e^{\frac{1}{4} \boldsymbol{\gamma}^T W_{\mathbf{s}} \boldsymbol{\gamma}}, \quad (\text{S17})$$

we obtain another expression of $\Gamma_{\mathbf{s}}$,

$$\Gamma_{\mathbf{s}, kl} = \text{Tr} \left[\rho_{\mathbf{s}} \frac{1}{4} \boldsymbol{\gamma}^T O^{kl} \boldsymbol{\gamma} \right] = \frac{\text{Tr} \left[e^{\frac{1}{4} \boldsymbol{\gamma}^T W_{\mathbf{s}} \boldsymbol{\gamma}} \frac{1}{4} \boldsymbol{\gamma}^T O^{kl} \boldsymbol{\gamma} \right]}{\text{Tr} \left[e^{\frac{1}{4} \boldsymbol{\gamma}^T W_{\mathbf{s}} \boldsymbol{\gamma}} \right]} = \left[(I + e^{W_{\mathbf{s}}})^{-1} e^{W_{\mathbf{s}}} \right]_{lk} - \left[(I + e^{W_{\mathbf{s}}})^{-1} e^{W_{\mathbf{s}}} \right]_{kl}. \quad (\text{S18})$$

Compare Eq. (S16) with Eq. (S18), we learn that $\tilde{F} \equiv -(I + e^W)^{-1}e^W$ (omit the auxiliary field subscripts \mathbf{s}) should be equal to F up to an arbitrary symmetric matrix. Based on the above relation, we can prove the relation between Γ and W ,

$$\begin{aligned}\Gamma &= \tilde{F} - \tilde{F}^T = -(I + e^W)^{-1}e^W + e^{-W}(I + e^{-W})^{-1} \\ &= -\left(e^{W/2} - e^{-W/2}\right)\left(e^{W/2} + e^{-W/2}\right)^{-1} = \tanh(-W/2).\end{aligned}\quad (\text{S19})$$

This relation is of importance because it indicates that a covariance matrix can be used to describe a Gaussian state equivalently.

The ‘‘partial transpose of the Green’s function’’ in Majorana basis is quite straightforward via Eq. (S6),

$$\Gamma^{T_2^f} = \begin{pmatrix} \Gamma^{11} & i\Gamma^{12} \\ i\Gamma^{21} & -\Gamma^{22} \end{pmatrix}, \quad (\text{S20})$$

where $\Gamma^{bb'}$ represents the block consisting of matrix elements with rows belonging to subsystem A_b and columns belonging to subsystem $A_{b'}$. At the moment, our understanding is limited to the fact that $\Gamma^{T_2^f}$ naturally represents a new Gaussian state, which can generally be expanded using Eq. (S5):

$$\rho' = \sum_{\kappa, \tau} w'_{\kappa, \tau} \gamma_{m_1}^{\kappa_1} \cdots \gamma_{m_{2k}}^{\kappa_{2k}} \gamma_{n_1}^{\tau_1} \cdots \gamma_{n_{2l}}^{\tau_{2l}}. \quad (\text{S21})$$

We can further use the Wick theorem for arbitrary Majorana monomial [S6] (i.e., products of $2l$ Majorana operators with index different from each other)

$$\text{Tr}(\rho \gamma_{n_1} \gamma_{n_2} \cdots \gamma_{n_{2l}}) = \sum_{\pi} \text{sgn}(\pi) \prod_{k=1}^l \Gamma_{n_{\pi(2k-1)}, n_{\pi(2k)}} \quad (\text{S22})$$

to identify the new Gaussian. Here, ρ is the Gaussian state associated with Γ , and π is a permutation representing different pairs of Majorana operators. On the one hand, we can take ρ' as the Majorana monomial

$$\text{Tr}(\rho \rho') = \sum_{\kappa, \tau} w'_{\kappa, \tau} \text{Tr}(\rho \gamma_{m_1}^{\kappa_1} \cdots \gamma_{m_{2k}}^{\kappa_{2k}} \gamma_{n_1}^{\tau_1} \cdots \gamma_{n_{2l}}^{\tau_{2l}}). \quad (\text{S23})$$

On the other hand, we can also use ρ' as the Gaussian state to expand ρ

$$\begin{aligned}\text{Tr}(\rho' \rho) &= \sum_{\kappa, \tau} w_{\kappa, \tau} \text{Tr}(\rho' \gamma_{m_1}^{\kappa_1} \cdots \gamma_{m_{2k}}^{\kappa_{2k}} \gamma_{n_1}^{\tau_1} \cdots \gamma_{n_{2l}}^{\tau_{2l}}) = \sum_{\kappa, \tau} w_{\kappa, \tau} \sum_{\pi} \text{sgn}(\pi) \prod_{p=1}^{k+l} (\Gamma^{T_2^f})_{\pi(2p-1), \pi(2p)} \\ &= \sum_{\kappa, \tau} w_{\kappa, \tau} i^{|\tau|} \sum_{\pi} \text{sgn}(\pi) \prod_{p=1}^{k+l} \Gamma_{\pi(2p-1), \pi(2p)} = \sum_{\kappa, \tau} w_{\kappa, \tau} i^{|\tau|} \text{Tr}(\rho \gamma_{m_1}^{\kappa_1} \cdots \gamma_{m_{2k}}^{\kappa_{2k}} \gamma_{n_1}^{\tau_1} \cdots \gamma_{n_{2l}}^{\tau_{2l}}).\end{aligned}\quad (\text{S24})$$

Upon comparing the two equations above, we observe that ρ' linked with $\Gamma^{T_2^f}$ is in fact the partially transposed Gaussian state $\rho^{T_2^f}$ (note that we have omitted the auxiliary field index in this paragraph).

In short, for each Gaussian state $\rho_{\mathbf{s}}$ associated with a specific configuration of the auxiliary field, its partial transpose can be expressed via the partial transpose of Green’s function in Eq. (S20), yields the following weighted sum formulation of the partially transposed density matrix

$$\rho^{T_2^f} = \sum_{\mathbf{s}} p_{\mathbf{s}} \rho_{\mathbf{s}}^{T_2^f}, \quad \rho_{\mathbf{s}}^{T_2^f} = \det \left[I + e^{W_{\mathbf{s}}^{T_2^f}} \right]^{-1/2} e^{\frac{1}{4} \gamma^T W_{\mathbf{s}}^{T_2^f} \gamma}, \quad (\text{S25})$$

where $W_{\mathbf{s}}^{T_2^f} = \ln[(I + \Gamma_{\mathbf{s}}^{T_2^f})^{-1}(I - \Gamma_{\mathbf{s}}^{T_2^f})]$. This formula can be re-expressed in the complex fermion basis, which is more convenient for practical calculations

$$\rho^{T_2^f} = \sum_{\mathbf{s}} p_{\mathbf{s}} \rho_{\mathbf{s}}^{T_2^f}, \quad \rho_{\mathbf{s}}^{T_2^f} = \det \left[G_{\mathbf{s}}^{T_2^f} \right] \exp \left\{ \mathbf{c}^\dagger \ln \left[\left(G_{\mathbf{s}}^{T_2^f} \right)^{-1} - I \right] \mathbf{c} \right\}, \quad (\text{S26})$$

where

$$G^{T_2^f} = \begin{pmatrix} G^{11} & iG^{12} \\ iG^{21} & I - G^{22} \end{pmatrix}. \quad (\text{S27})$$

ADDITIONAL RESULTS OF THE RÉNYI NEGATIVITY

For a more direct comprehension of the distinction between Rényi negativity and Rényi entropy, one can see Fig. S1. In this figure, we compare the Rényi entropy S_2 , the Rényi negativity \mathcal{E}_2 , and the Rényi negativity ratio R_2 for a half-filled Hubbard chain. The $S_2 - L_{A_1}$ curve in Fig. S1(a) resembles the findings of previous studies (e.g., see Ref. [S17]). As the temperature rises, the Rényi entropy S_2 experiences a quantum-classical transition, shifting from an area law (inclusive of a logarithmic correction) at zero-temperature to a volume law $S_2 = L_{A_1} \log 4$ in the high-temperature limit. At finite temperatures, while the $S_2 - L_{A_1}$ curve exhibits asymmetry about $L_{A_1} = L/2$, the Rényi negativity (see Fig. S1(b)) maintains an arc-like structure. Moreover, the two endpoints of the $\mathcal{E}_2 - L_{A_1}$ curve correspond to the thermal entropy $S_2^{\text{th}} = S_2(L_{A_1} = L) = \mathcal{E}_2(L_{A_1} = 0) = \mathcal{E}_2(L_{A_1} = L) = -\ln(\text{Tr}[\rho^2])$. Upon subtracting the thermal entropy from \mathcal{E}_2 , the negativity ratio R_2 (see Fig. S1(c)) emerges as a more capable indicator of finite-temperature entanglement, given its monotonic decrease with rising temperature. In the high-temperature limit, the $R_2 - L_{A_1}$ curve becomes flat for bulk L_{A_1} values. This plateau can be well described by the formula $\mathcal{E}(LT \gg 1) = \frac{1}{2} \left[\ln \left| \frac{\beta}{\pi} \sinh \left(\frac{\pi L_{A_1}}{\beta} \right) \right| - \frac{\pi L_{A_1}}{\beta} \right] + O(e^{-\pi LT})$ obtained by conformal field theory [S3] and reflects the area law.

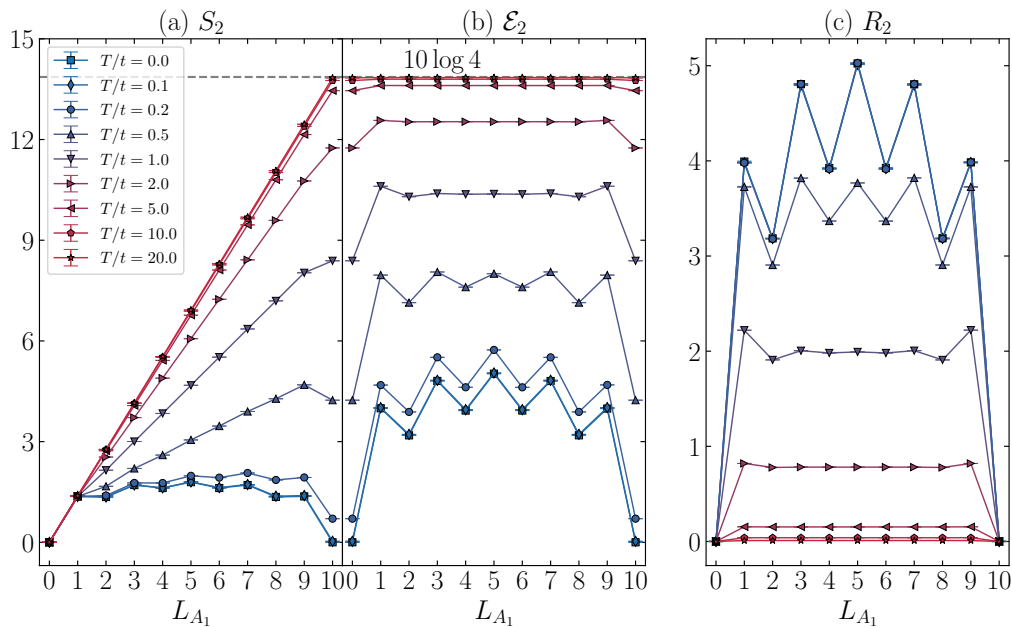


FIG. S1. The comparison of the Rényi entanglement entropy S_2 , the Rényi negativity \mathcal{E}_2 , and the Rényi negativity ratio R_2 as functions of the subsystem size L_{A_1} is presented for a half-filled Hubbard chain with a length of $L = 10 (= L_{A_1} + L_{A_2})$ at various temperatures. The dashed line signifies the thermal entropy in the limit as T approaches infinity, represented by $S_2^{\text{th}}(T \rightarrow \infty) = L_{A_1} \log 4$ [S17].

As shown in Fig. S2, the super-area-law feature near the finite-temperature critical point of the t - V model is evident for two different values of V , a different lattice, and a different bipartition geometry. Figs. S2(a) and (b) show the cases with interaction strengths $V/t = 1.0$ and $V/t = 0.0$ (free fermion case), respectively. The bipartition geometry remains the same as that in Fig. 3 of the main text and is indicated by the right inset of Fig. S2(a). In the $V/t = 1.0$ case, the peak of R_2/L is located at $T = 0.833t \approx 2T_c$, aligning with prior findings of $T_c/t \approx 0.4 \pm 0.1$ obtained by DQMC [S18]. In the free fermion case, since $T = 0$ is the critical point, the $L \ln L$ scaling is observed at low temperatures, likely associated with the entanglement entropy of the Fermi surface [S19] as previous studies on negativity stated [S3, S20]. Surprisingly, this scaling persists to a considerable extent at higher temperatures, indicating a prolonged crossover. Fig. S2(c) depicts the scenarios with $V/t = 2.0$ on a honeycomb lattice. The super-area-law feature is still evident, and the maximum of R_2/L is observed at $T = 1.111t \approx 2T_c$, which is slightly higher than the previous result of $T_c/t \approx 0.472$ obtained by continuous-time QMC [S21]. Fig. S2(d) presents the case with an equal bipartition geometry on a square lattice. Despite the subpar data quality, the super-area-law feature around the same critical point as the quarter bipartition case is also observed.

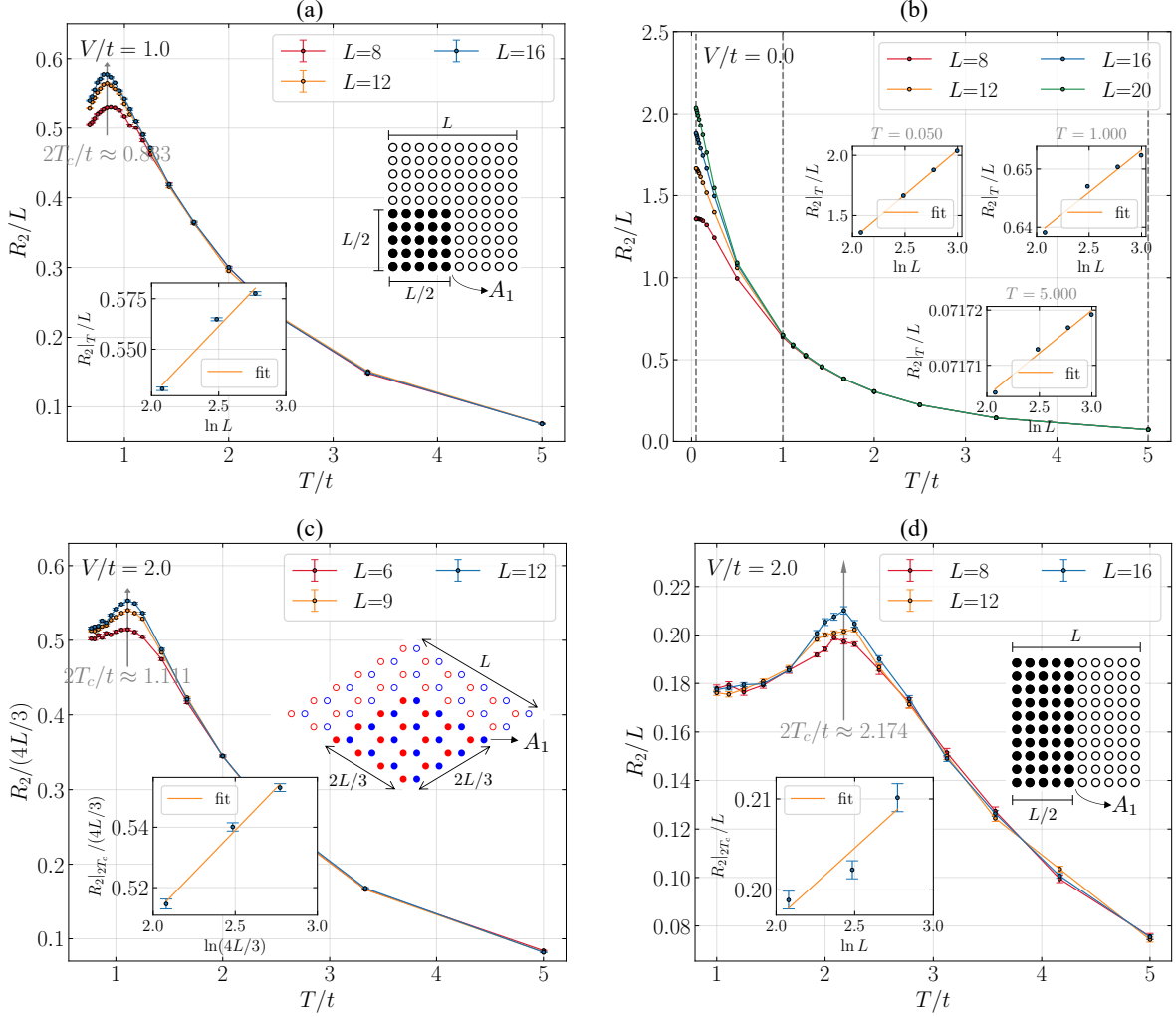


FIG. S2. The area-law coefficients of the Rényi negativity ratio R_2 as functions of temperature for the t - V model. A super-area-law feature around the finite-temperature critical point is evident for (a) $V/t = 1.0$, (b) $V/t = 0$ (free fermion case), (c) $V/t = 2.0$ on a honeycomb lattice and (d) equal-bipartition geometry. In Figs. (a) and (b), the bipartition geometry matches that of Fig. 3 in the main text, as indicated by the right inset of Fig. (a).

SIGN PROBLEM OF GROVER DETERMINANT

Using the expression for $\rho_{\mathbf{s}}^{T_2^f}$, we can calculate rank- n Rényi negativity within DQMC framework,

$$\begin{aligned}
 e^{-(n-1)\mathcal{E}_n} &= \text{Tr} \left[\left(\rho_{\mathbf{s}_2}^{T_2^f} \right)^n \right] = \sum_{\mathbf{s}_1 \dots \mathbf{s}_n} P_{\mathbf{s}_1} \dots P_{\mathbf{s}_n} \text{Tr} \left[\rho_{\mathbf{s}_1}^{T_2^f} \dots \rho_{\mathbf{s}_n}^{T_2^f} \right] \\
 &= \sum_{\mathbf{s}_1 \dots \mathbf{s}_n} P_{\mathbf{s}_1} \dots P_{\mathbf{s}_n} \det g_x^n = \langle \det g_x^n \rangle,
 \end{aligned} \tag{S28}$$

where we have defined the so-called *Grover matrix* g_x^n

$$g_x^n = G_{\mathbf{s}_1}^{T_2^f} \dots G_{\mathbf{s}_n}^{T_2^f} \left[I + \left(G_{\mathbf{s}_1}^{T_2^f} \right)^{-1} \left(I - G_{\mathbf{s}_1}^{T_2^f} \right) \dots \left(G_{\mathbf{s}_n}^{T_2^f} \right)^{-1} \left(I - G_{\mathbf{s}_n}^{T_2^f} \right) \right] \tag{S29}$$

and its determinant $\det g_x^n$ called *Grover determinant*. As an entanglement measurement, $\mathcal{E}_n \geq 0$ so that $0 < \langle \det g_x^n \rangle \leq 1$. It is an interesting question whether for any specific configuration of auxiliary fields $\{\mathbf{s}_1, \dots, \mathbf{s}_n\}$, we always have $\det g_x^n \geq 0$. Moreover, this condition is necessary for the development of an incremental algorithm [S11, S12] that can

accurately compute Rényi negativity, as the weights of all incremental processes include a factor of $(\det g_x^n)^{1/N}$. In this section, we prove that the Grover determinant is real and positive for two classes of sign-problem-free models. We note that these conditions are also applicable to the corresponding Grover determinant associated with entanglement entropy, where all the $G^{T_2^f}$ in Eq. (S29) are replaced by G^{A_2} . We only consider models on bipartite lattices and use the notion $(-)^i$ for staggered phase factor that takes 1 (-1) at sites belonging to sublattice A (B).

$$\text{Sufficient Condition I: } G_{ij}^\downarrow = (-)^{i+j}(\delta_{ij} - G_{ji}^{\uparrow*})$$

The first class of models includes the half-filled Hubbard model on bipartite lattices. After HS transformation that decouples Hubbard term to density channel as in Eq. (S8), the spacetime-dependent Hamiltonian for a specific configuration of auxiliary fields is given by

$$H = \sum_i iC_i(n_{i\uparrow} + n_{i\downarrow} - 1) + \sum_{\langle i,j \rangle} D_{ij}(c_{i\uparrow}^\dagger c_{j\uparrow} + c_{i\downarrow}^\dagger c_{j\downarrow} + \text{h.c.}), \quad (\text{S30})$$

where C_i and D_{ij} are real constant factors. Turn to a new basis via a partial particle-hole transformation $\tilde{c}_{i\uparrow} = c_{i\uparrow}$, $\tilde{c}_{i\downarrow} = (-)^i c_{i\downarrow}^\dagger$, we obtain

$$\tilde{H} = \sum_i iC_i(\tilde{n}_{i\uparrow} - \tilde{n}_{i\downarrow}) + \sum_{\langle i,j \rangle} D_{ij}(\tilde{c}_{i\uparrow}^\dagger \tilde{c}_{j\uparrow} + \tilde{c}_{i\downarrow}^\dagger \tilde{c}_{j\downarrow} + \text{h.c.}) \quad (\text{S31})$$

This Hamiltonian possesses an anti-unitary symmetry $i\sigma_y \mathcal{K}$, where σ_y acts on the spin sector and \mathcal{K} means complex conjugate, so it is sign-problem-free. Since the blocks in spin-up and spin-down sectors are complex conjugate to each other, $\tilde{H}_\uparrow = \tilde{H}_\downarrow$, the two blocks in any eigenvector of Hamiltonian and hence the Green's function are also complex conjugate to each other, $\tilde{G}_{ij}^\downarrow \equiv \langle \tilde{c}_{i\downarrow} \tilde{c}_{j\downarrow}^\dagger \rangle = \tilde{G}_{ij}^{\uparrow*} \equiv \langle \tilde{c}_{i\uparrow} \tilde{c}_{j\uparrow}^\dagger \rangle$. Return to the original basis, we find that the Green's functions satisfy the following relation

$$G_{ij}^\downarrow = (-)^{i+j}(\delta_{ij} - G_{ji}^{\uparrow*}), \quad (\text{S32})$$

which can be rewritten as the following matrix form

$$G^\downarrow = U^\dagger (I - (G^\uparrow)^\dagger) U \quad (\text{S33})$$

with $U_{ij} = \delta_{ij}(-)^i = \delta_{ij}(-)^j$ a diagonal unitary matrix.

The condition in Eq. (S32) is sufficient for $\det g_x^n \geq 0$. Consider the spin-up block of partially transposed Green's function in Eq. (S27), which satisfies

$$U^\dagger (G^{\uparrow, T_2^f})^\dagger U = V G^{\downarrow, T_2^f} V + I, \quad \text{with } V = \begin{pmatrix} iI_1 & \\ & -iI_2 \end{pmatrix}. \quad (\text{S34})$$

V is a diagonal unitary matrix satisfying $V^2 = -I$. Reformulate the above relation we have

$$\begin{aligned} G^{\downarrow, T_2^f} &= V^\dagger U^\dagger \left(I - (G^{\uparrow, T_2^f})^\dagger \right) UV, \\ I - G^{\uparrow, T_2^f} &= UV \left(G^{\downarrow, T_2^f} \right)^\dagger V^\dagger U^\dagger, \\ 1 - G^{\downarrow, T_2^f} &= V^\dagger U^\dagger \left(G^{\uparrow, T_2^f} \right)^\dagger UV. \end{aligned} \quad (\text{S35})$$

Using the above relations, one can prove that $\det g_x^n = \det g_x^{n,\uparrow} \det g_x^{n,\downarrow} \geq 0$ since

$$\begin{aligned} \det g_x^{n,\downarrow} &\equiv \det \left\{ G_{\mathbf{s}_1}^{\downarrow, T_2^f} \cdots G_{\mathbf{s}_n}^{\downarrow, T_2^f} \left[I + \left(G_{\mathbf{s}_1}^{\downarrow, T_2^f} \right)^{-1} \left(I - G_{\mathbf{s}_1}^{\downarrow, T_2^f} \right) \cdots \left(G_{\mathbf{s}_n}^{\downarrow, T_2^f} \right)^{-1} \left(I - G_{\mathbf{s}_n}^{\downarrow, T_2^f} \right) \right] \right\} \\ &= \det \left\{ \left[I + G_{\mathbf{s}_n}^{\uparrow, T_2^f} \left(I - G_{\mathbf{s}_n}^{\uparrow, T_2^f} \right)^{-1} \cdots G_{\mathbf{s}_1}^{\uparrow, T_2^f} \left(I - G_{\mathbf{s}_1}^{\uparrow, T_2^f} \right)^{-1} \right] \left(I - G_{\mathbf{s}_n}^{\uparrow, T_2^f} \right) \cdots \left(I - G_{\mathbf{s}_1}^{\uparrow, T_2^f} \right) \right\}^* \\ &= \det \left\{ G_{\mathbf{s}_1}^{\uparrow, T_2^f} \cdots G_{\mathbf{s}_n}^{\uparrow, T_2^f} \left[I + \left(G_{\mathbf{s}_1}^{\uparrow, T_2^f} \right)^{-1} \left(I - G_{\mathbf{s}_1}^{\uparrow, T_2^f} \right) \cdots \left(G_{\mathbf{s}_n}^{\uparrow, T_2^f} \right)^{-1} \left(I - G_{\mathbf{s}_n}^{\uparrow, T_2^f} \right) \right] \right\}^* \\ &\equiv (\det g_x^{n,\uparrow})^*. \end{aligned} \quad (\text{S36})$$

Sufficient Condition II: $\Gamma_{ij}^{(2)} = (-)^{i+j} \Gamma_{ij}^{(1)*}$

The second class of models, including the spinless t - V model on bipartite lattices, are proved in Majorana basis. For convenience, let us first relabel the Majorana operators by introducing a specie index, i.e., we use $\gamma_i^{(1)}$ and $\gamma_i^{(2)}$ to represent γ_{2i-1} and γ_{2i} , respectively. After HS transformation that decouples NN interaction terms to Majorana hopping channel as in Eq. (S9), the spacetime-dependent Hamiltonian for a specific configuration of auxiliary fields is given by

$$H = \sum_{\langle ij \rangle} C_{ij} \left(i\gamma_i^{(1)}\gamma_j^{(1)} + i\gamma_i^{(2)}\gamma_j^{(2)} \right), \quad (\text{S37})$$

where C_i are real constant factors. This Hamiltonian possesses an anti-unitary symmetry $T\mathcal{K}$, where T transforms $\gamma_i^{(1)}$ ($\gamma_i^{(2)}$) to $(-)^i\gamma_i^{(2)}$ ($(-)^i\gamma_i^{(1)}$), so it is sign-problem-free. Turn to a new basis via transformation $\tilde{\gamma}_i^{(1)} = \gamma_i^{(1)}$, $\tilde{\gamma}_i^{(2)} = (-)^i\gamma_i^{(2)}$, the Hamiltonian becomes

$$\tilde{H} = \sum_{\langle ij \rangle} C_{ij} \left(i\tilde{\gamma}_i^{(1)}\tilde{\gamma}_j^{(1)} - i\tilde{\gamma}_i^{(2)}\tilde{\gamma}_j^{(2)} \right). \quad (\text{S38})$$

Since the coefficients of $\tilde{\gamma}_i^{(1)}\tilde{\gamma}_j^{(1)}$ and $\tilde{\gamma}_i^{(2)}\tilde{\gamma}_j^{(2)}$ are complex conjugate to each other, using similar arguments as the case of Hubbard model, we have the relation $\tilde{\Gamma}^{(2)} = \tilde{\Gamma}^{(1)*}$. Return to the original basis, we find that Green's functions satisfy the following relation

$$\Gamma_{ij}^{(2)} = (-)^{i+j}\Gamma_{ij}^{(1)*} \text{ or } \Gamma^{(2)} = U^\dagger \Gamma^{(1)*} U. \quad (\text{S39})$$

The condition stated in Eq. (S39) is also sufficient for $\det g_x^n \geq 0$. According to the expression of partially transposed Green's function in Eq. (S20) and $W^{T_2^f} = \ln[(I + \Gamma^{T_2^f})^{-1}(I - \Gamma^{T_2^f})]$, we can derive the relationships between the two blocks pertaining to two distinct Majorana species sectors:

$$\Gamma^{(2), T_2^f} = J^\dagger U^\dagger \left(\Gamma^{(1), T_2^f} \right)^* U J \text{ and } W^{(2), T_2^f} = J^\dagger U^\dagger \left(W^{(1), T_2^f} \right)^* U J \text{ with } J = \begin{pmatrix} I_1 & \\ & -I_2 \end{pmatrix}. \quad (\text{S40})$$

Write the Grover determinant in Majorana basis using Eq. (S25), and it can be easily proved that $\det g_x^n = \det g_x^{n,(1)} \det g_x^{n,(2)} \geq 0$ since

$$\begin{aligned} \det g_x^{n,(2)} &= \det \left[I + e^{W_{s_1}^{(2), T_2^f}} \right]^{-1/2} \cdots \det \left[I + e^{W_{s_n}^{(2), T_2^f}} \right]^{-1/2} \det \left[I + e^{W_{s_1}^{(2), T_2^f}} \cdots e^{W_{s_n}^{(2), T_2^f}} \right]^{1/2} \\ &= \det \left[I + e^{W_{s_1}^{(1), T_2^f, *}} \right]^{-1/2} \cdots \det \left[I + e^{W_{s_n}^{(1), T_2^f, *}} \right]^{-1/2} \det \left[I + e^{W_{s_1}^{(1), T_2^f, *}} \cdots e^{W_{s_n}^{(1), T_2^f, *}} \right]^{1/2} \\ &= \det g_x^{n,(1)*}. \end{aligned} \quad (\text{S41})$$

* xiaoyanxu@sjtu.edu.cn

- [S1] G. Vidal and R. F. Werner, Computable measure of entanglement, *Physical Review A* **65**, 032314 (2002).
- [S2] K. Shiozaki, H. Shapourian, K. Gomi, and S. Ryu, Many-body topological invariants for fermionic short-range entangled topological phases protected by antiunitary symmetries, *Physical Review B* **98**, 035151 (2018).
- [S3] H. Shapourian and S. Ryu, Finite-temperature entanglement negativity of free fermions, *Journal of Statistical Mechanics: Theory and Experiment* **2019**, 043106 (2019).
- [S4] E. Fradkin, Disorder Operators and Their Descendants, *Journal of Statistical Physics* **167**, 427 (2017).
- [S5] Z. H. Liu, Y. D. Liao, G. Pan, M. Song, J. Zhao, W. Jiang, C.-M. Jian, Y.-Z. You, F. F. Assaad, Z. Y. Meng, and C. Xu, Disorder Operator and Renyi Entanglement Entropy of Symmetric Mass Generation, *Physical Review Letters* **132**, 156503 (2024).
- [S6] V. Eisler and Z. Zimborás, On the partial transpose of fermionic Gaussian states, *New Journal of Physics* **17**, 053048 (2015).
- [S7] H. Shapourian, K. Shiozaki, and S. Ryu, Partial time-reversal transformation and entanglement negativity in fermionic systems, *Physical Review B* **95**, 165101 (2017).

- [S8] F. Assaad and H. Evertz, World-line and Determinantal Quantum Monte Carlo Methods for Spins, Phonons and Electrons, in *Computational Many-Particle Physics*, Lecture Notes in Physics, edited by H. Fehske, R. Schneider, and A. Weiße (Springer, Berlin, Heidelberg, 2008) pp. 277–356.
- [S9] Z.-X. Li, Y.-F. Jiang, and H. Yao, Solving the fermion sign problem in quantum Monte Carlo simulations by Majorana representation, *Physical Review B* **91**, 241117 (2015).
- [S10] F. Sun and X. Y. Xu, [Delay Update in Determinant Quantum Monte Carlo](#) (2023), [arxiv:2308.12005 \[cond-mat\]](#).
- [S11] Y. D. Liao, G. Pan, W. Jiang, Y. Qi, and Z. Y. Meng, The teaching from entanglement: 2D SU(2) antiferromagnet to valence bond solid deconfined quantum critical points are not conformal (2023), [arxiv:2302.11742 \[cond-mat, physics:math-ph, physics:physics, physics:quant-ph\]](#).
- [S12] In preparation.
- [S13] G. H. Lang, C. W. Johnson, S. E. Koonin, and W. E. Ormand, Monte Carlo evaluation of path integrals for the nuclear shell model, *Physical Review C* **48**, 1518 (1993).
- [S14] I. Klich, A note on the full counting statistics of paired fermions, *Journal of Statistical Mechanics: Theory and Experiment* **2014**, P11006 (2014).
- [S15] Z.-C. Wei, [Semigroup Approach to the Sign Problem in Quantum Monte Carlo Simulations](#) (2018), [arxiv:1712.09412 \[cond-mat, physics:hep-lat, physics:math-ph, physics:nucl-th\]](#).
- [S16] T. Grover, Entanglement of Interacting Fermions in Quantum Monte Carlo Calculations, *Physical Review Letters* **111**, 130402 (2013).
- [S17] P. Broecker and S. Trebst, Rényi entropies of interacting fermions from determinantal quantum Monte Carlo simulations, *Journal of Statistical Mechanics: Theory and Experiment* **2014**, P08015 (2014).
- [S18] D. J. Scalapino, R. L. Sugar, and W. D. Toussaint, Monte Carlo study of a two-dimensional spin-polarized fermion lattice gas, *Physical Review B* **29**, 5253 (1984).
- [S19] B. Swingle, Entanglement Entropy and the Fermi Surface, *Physical Review Letters* **105**, 050502 (2010).
- [S20] V. Eisler and Z. Zimborás, Entanglement negativity in two-dimensional free lattice models, *Physical Review B* **93**, 115148 (2016).
- [S21] S. Hesselmann and S. Wessel, Thermal Ising transitions in the vicinity of two-dimensional quantum critical points, *Physical Review B* **93**, 155157 (2016).